(112–408) and *in vitro* translated ^{35}S-labeled p73α, p73β, p73α(1–548) or p53. GST alone was employed as a negative control. As shown in Figure 1c, radio-labeled p73α was pulled down by GST-RanBPM(112–408) but not by GST alone. However, p73β and p73α(1–548), which lack the extreme COOH-terminal portion of p73α, were no longer able to interact with GST-RanBPM(112–408). In addition, p53 failed to bind to GST-RanBPM(112–408). In good agreement with the yeast two-hybrid results, these observations suggest that the extreme COOH-terminal portion of p73α is responsible for the physical interaction with RanBPM. Next, we performed co-immunoprecipitation experiments to confirm their interaction in cells. To this end, cell lysates prepared from COS7 cells co-transfected with HA-tagged p73α and FLAG-tagged full-length RanBPM were immunoprecipitated with anti-p73 or anti-FLAG antibody, followed by immunoblotting with anti-FLAG or anti-HA antibody, respectively. As shown in Figure 1d, HA-p73α co-immunoprecipitated with FLAG-RanBPM. Under our experimental conditions, HA-p73α(1–427) and HA-p73α(1–247) did not co-immunoprecipitate with FLAG-RanBPM (Figure 1e). In contrast to full-length p73α, the anti-p53 immunoprecipitates did not contain FLAG-RanBPM (Figure 1f). Taken together, our results suggest that RanBPM has an ability to interact with p73α but not with p53 in mammalian cultured cells.

Previous immunostaining studies have shown that p73α is exclusively localized in cell nucleus (Jost *et al.*, 1997), while RanBPM could distribute to the cell nucleus, perinuclear region and cytoplasm (Nishitani *et al.*, 2001; Umeda *et al.*, 2003). To examine the subcellular localization of RanBPM in the presence or absence of p73α, COS7 cells were transfected with the indicated expression plasmids, and the indirect immunofluorescent staining was performed. As shown in Figure 2a and b, FLAG-RanBPM and HA-p73α were detected largely in the cytoplasm and cell nucleus, respectively. Of note, when FALG-RanBPM was co-expressed with HA-p73α, a fraction of FLAG-RanBPM translocated into cell nucleus, and co-localized with nuclear HA-p73α (Figure 2c–e). To confirm this issue, transfected COS7 cells were fractionated into nuclear and cytoplasmic fractions, and their subcellular localizations were analysed by immunoblotting. The purity of the nuclear and cytoplasmic fractions was examined by immunoblotting with anti-Lamin B and anti-α-tubulin antibody, respectively. Consistent with the indirect immunofluorescent staining, co-expression of FLAG-RanBPM with HA-p73α resulted in a significant nuclear accumulation of FLAG-RanBPM, whereas FLAG-RanBPM alone was detected in the cytoplasmic fraction (Figure 2f). In addition, the amounts of nuclear HA-p73α seemed to be increased in the presence of FLAG-RanBPM. It is thus likely that RanBPM interacts with p73α in cell nucleus, and could affect the stability of p73α.

To test whether RanBPM could affect the stability of p73α, COS7 cells were co-transfected with the constant amount of HA-p73α together with or without the

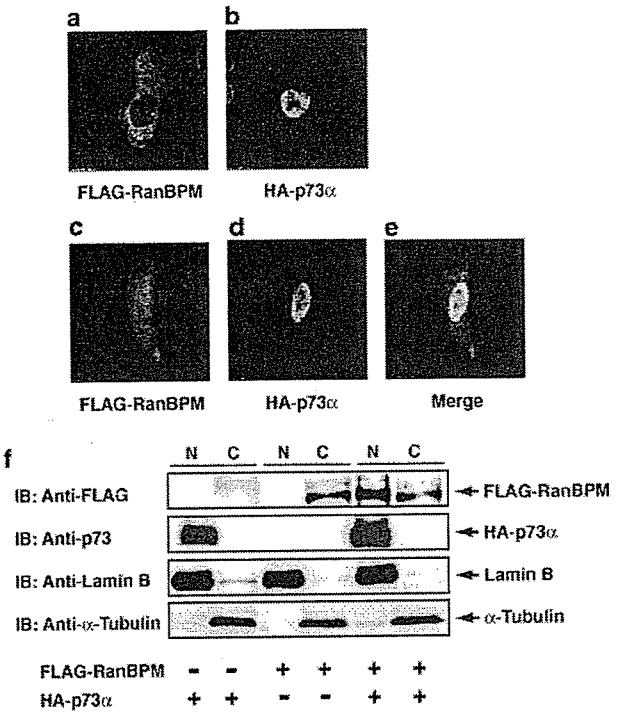

Figure 2 Subcellular distribution of RanBPM in the presence of p73. (a–e) Nuclear co-localization of p73α and RanBPM by immunofluorescence. COS7 cells were transfected with FLAG-RanBPM (a), HA-p73α (b) or FLAG-RanBPM and HA-p73α (c–e). At 48 h after transfection, cells were fixed in 20% methanol and incubated with anti-FLAG (red) and anti-HA antibody (green) (Medical and Biological Laboratories, Nagoya, Japan), followed by the incubation with the rhodamine- and FITC-conjugated secondary antibodies (Jackson ImmunoResearch Laboratories), respectively. Cells were then examined under a confocal scanning laser microscope. The merged images of the two signals are displayed in yellow (e). (f) Fractionation of COS7 cell extracts. COS7 cells were transfected with the indicated expression plasmids. At 48 h after transfection, cells were fractionated into nuclear (N) and cytoplasmic (C) fractions, and then analysed directly by immunoblotting with anti-FLAG (first panel) or anti-p73 antibody (second panel). The nuclear or cytoplasmic fraction was confirmed by immunoblotting with anti-Lamin B (Ab-1, Oncogene Research Products) (third panel) or anti-α-tubulin antibody (DM1A, Cell Signaling Technology, Beverly, MA, USA) (fourth panel), respectively

increasing amounts of FLAG-RanBPM. As shown in Figure 3a, the amount of HA-p73α was markedly increased in the presence of FLAG-RanBPM in a dose-dependent manner, whereas the expression level of p73α mRNA remained unchanged. On the other hand, FLAG-RanBPM had no significant effect on the levels of exogenous p53 (Figure 3b). Similar results were also obtained in p53-deficient H1299 cells (data not shown). We next sought to determine the half-life of p73α in the presence of RanBPM. For this purpose, COS7 cells were transfected with HA-p73α together with or without FLAG-RanBPM. At 24 h after transfection, cells were treated with cycloheximide. At the indicated time periods, cell lysates were analysed for HA-p73α by immunoblotting. In accordance with the previous reports (Lee and La Thangue, 1999; Ohtsuka *et al.*,

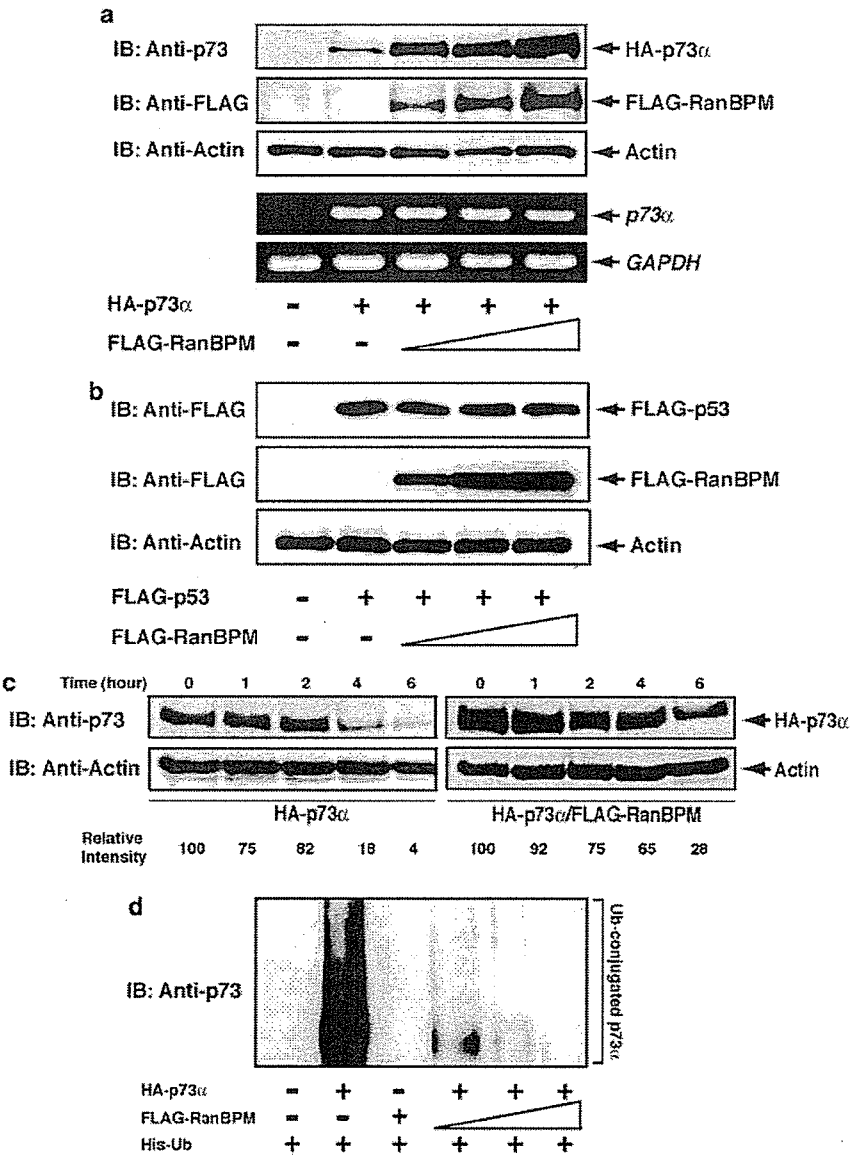

Figure 3 RanBPM increases the stability of p73 but not of p53. (**a**) RanBPM increases the amounts of p73α. COS7 cells were co-transfected with the constant amount of HA-p73α (0.5 μg) together with or without the increasing amounts of FLAG-RanBPM (0.5, 1.0 and 1.5 μg). The total amount of plasmid DNA was kept constant (2 μg) with pcDNA3. At 48 h after transfection, cell lysates or total RNA were prepared, and subjected to immunoblotting with the indicated antibodies (upper panels) or RT–PCR analysis (lower panels). Immunoblotting for actin (20–33, Sigma Chemical Co.) serves as a loading control. (**b**) RanBPM does not affect the amounts of p53. COS7 cells were co-transfected with the indicated combinations of the expression plasmids, and were processed for immunoblotting as described above. (**c**) RanBPM increases the half-life of p73α. COS7 cells were transfected with HA-p73α alone (0.5 μg) (left panels) or together with FLAG-RanBPM (1.5 μg) (right panels). At 24 h post-transfection, cells were treated with cycloheximide (100 μg/ml) and harvested at the indicated time periods. Cell lysates were used for immunoblotting with the indicated antibodies. The intensity of the bands was quantified by using densitometry. (**d**) RanBPM inhibits the ubiquitination of p73α. COS7 cells were co-transfected with the constant amount of HA-p73α (0.5 μg) and His-tagged ubiquitin (Ub) (0.5 μg), together with or without the increasing amounts of FLAG-RanBPM (0.5, 1.0 and 1.5 μg). At 24 h post-transfection, cells were treated with 20 μM MG-132 for 6 h before being harvested. His-tagged ubiquitin-containing protein complexes were pulled down with Ni^{2+}-agarose beads (QIAGEN, Valencia, CA, USA), and subsequently resolved by 10% SDS–polyacrylamide gel electrophoresis, followed by immunoblotting with anti-p73 antibody

2003), ectopically expressed p73α had a half-life of less than 4 h, whereas the degradation rate of HA-p73α was slower in FLAG-RanBPM-expressing cells (Figure 3c). Thus, it is likely that the RanBPM-dependent stabilization of p73α is attributed to the clear increase in the half-life of p73α.

As described (Balint *et al*., 1999), the stability of p73 is regulated at least in part through the ubiquitin–proteasome pathway. These observations prompted us to determine whether RanBPM could prevent the ubiquitination of p73. COS7 cells were transfected with HA-p73α- and His-tagged ubiquitin, or in combination

with the increasing amounts of FLAG-RanBPM. At 24 h after transfection, cells were treated with MG-132 for 6 h. His-ubiquitinated proteins were purified by Ni^{2+}-agarose beads, and then analysed by immunoblotting with the anti-p73 antibody. As shown in Figure 3d, the slower migrating ubiquitinated forms of p73α were detectable in the absence of FLAG-RanBPM. Intriguingly, the ubiquitination levels of p73α were significantly reduced in cells expressing FLAG-RanBPM, suggesting that RanBPM stabilizes p73α by inhibiting its ubiquitination.

To determine whether RanBPM could affect the transcriptional activity of p73α, H1299 cells were transiently transfected with a constant amount of the expression plasmid for HA-p73α, together with the p53/p73-responsive $p21^{WAF1}$ or *MDM2* luciferase reporter constructs in the presence or absence of increasing amounts of the FLAG-RanBPM expression plasmid. As shown in Figure 4a, expression of FLAG-RanBPM enhanced the ability of p73α to transactivate the $p21^{WAF1}$ and *MDM2* promoters in a dose-dependent manner. To extend the functional significance of their interaction, we examined the possible effect of RanBPM on the p73α-mediated apoptosis. H1299 cells were transfected with HA-p73α, FLAG-RanBPM, or HA-p73α and FLAG-RanBPM. The β-galactosidase was used as a marker to visualize the transfected cells. At 48 h post transfection, the number of β-galactosidase-positive cells was scored. As shown in Figure 4b, the number of β-galactosidase-positive cells expressing FLAG-RanBPM was similar to that detected in the empty plasmid-transfected cells. Consistent with the previous report (Watanabe *et al.*, 2002), expression of HA-p73α resulted in a clear decrease in the number of β-galactosidase-positive cells. Of note, co-expression of HA-p73α with FLAG-RanBPM significantly reduced the number of β-galactosidase-positive cells as compared with that observed in cells expressing HA-p73α alone. In addition, we performed a colony formation assay. H1299 cells were transfected with HA-p73α, FLAG-RanBPM or HA-p73α plus FLAG-RanBPM, and the transfected cells were selected in the presence of G418. After 2 weeks of selection, drug-resistant colonies were fixed and stained with Giemsa's solution. In accordance with the β-galactosidase assay, FLAG-RanBPM expression did not affect the colony formation as compared with the empty plasmid-transfected control, whereas co-expression of HA-p73α with FLAG-RanBPM reduced the colony formation even more efficiently than HA-p73α alone (Figure 4c). Considering that p73α efficiently induced apoptosis in H1299 cells (Di Como *et al.*, 1999; Zeng *et al.*, 1999), these results suggest that RanBPM increases the proapoptotic activity of p73α. To further confirm this issue, H1299 cells were transiently transfected with a constant amount of the GFP expression plasmid along with the indicated combinations of the expression plasmids. At 48 h after transfection, transfected cells were identified by fluorescence microscopy for the appearance of green fluorescence, and the number of GFP-positive cells with condensed and fragmented nuclei was counted. As shown in Figure 4d, co-expression of HA-p73α with FLAG-RanBPM increased the number of apoptotic cells as compared with that resulting from expression of HA-p73α alone. Taken together, our present results strongly suggest that RanBPM-mediated stabilization of p73α is critical for its effects on transcriptional activation as well as apoptosis.

Recently, it has been shown that a variety of cellular proteins could interact with RanBPM, including MET, androgen receptor, HIPK2, USP11, Twa1, calbindin D28K and $p75^{NTR}$, suggesting that RanBPM is involved in diverse biological processes (Ideguchi *et al.*, 2002; Rao *et al.*, 2002; Wang D *et al.*, 2002; Wang Y *et al.*, 2002; Bai *et al.*, 2003; Lutz *et al.*, 2003; Umeda *et al.*, 2003). In the present study, we demonstrated that RanBPM increased the stability of p73α by reducing its ubiquitination levels. An important question raised by our results is how RanBPM stabilize p73α. Intriguingly, Ideguchi *et al.* (2002) described that RanBPM is associated with the deubiquitination enzyme USP11, which belongs to the ubiquitin hydrolase family. Considering that p53 is stabilized by direct deubiquitination by the deubiquitination enzyme HAUSP (Li *et al.*, 2002), it is likely that RanBPM could bind to USP11 and promote deubiquitination of p73α by recruiting USP11 to p73α; however, further studies will be required to determine this issue.

Alternatively, Lee and La Thangue (1999) found that p73β is much more stable than p73α, suggesting that the unique COOH-terminal portion of p73α might be critical for degradation by the ubiquitin–proteasome system. According to our present results, RanBPM bound to p73α through its extreme COOH-terminal region, whereas it failed to interact with p73β. Thus, it is plausible that RanBPM might increase the steady-state levels of p73α by masking p73α COOH-terminal lysine residues, which could be the sites for ubiquitin ligation, and/or disrupting the interaction of p73α with unknown proteins required for ubiquitination-mediated proteolysis. These possibilities are currently under investigation. Elucidation of the detailed molecular mechanism underlying the RanBPM-dependent stabilization of p73α would be necessary for better understanding of p73 turnover.

Another finding of the present study is that, under our experimental conditions, cytoplasmic RanBPM became nuclear in the presence of p73α overexpression. Given that RanBPM is localized in both the cytoplasm and nucleus (Nakamura *et al.*, 1998; Nishitani *et al.*, 2001), it is probable that p73α might have an ability to promote nuclear translocation of RanBPM through the physical interaction between them. As described previously, wild-type p53 is predominantly localized in the cytoplasm of many neuroblastoma cells (Moll *et al.*, 1996). The abnormal cytoplasmic distribution of p53 might be attributed at least in part to the interaction with Parc, which acts as a cytoplasmic anchor protein for p53 (Nikolaev *et al.*, 2003). Interestingly, Goldschneider *et al.* (2004) found that enforced expression of p73α in neuroblastoma-derived SH-SY5Y cells significantly enhances the nuclear accumulation of wild-type p53 and

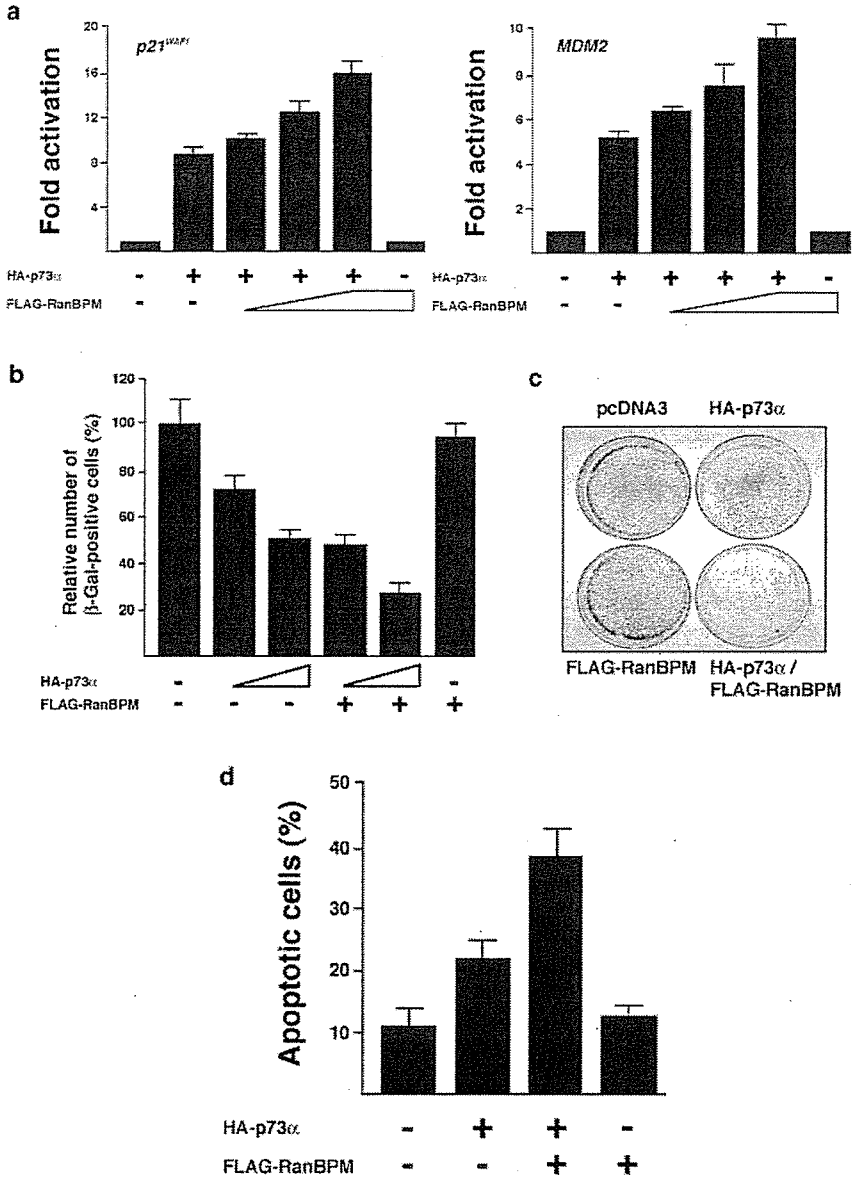

Figure 4 RanBPM enhances p73 function. (**a**) RanBPM enhances the transcriptional activity of p73α. p53-deficient H1299 cells were co-transfected with 25 ng of the expression plasmid for HA-p73α together with 100 ng of p53/p73-responsive *p21*^{WAF1} (left panel) or *MDM2* (right panel) luciferase reporter construct, and 10 ng of the *Renilla* luciferase plasmid (pRL-TK, Promega Corp., Madison, WI, USA), in the presence or absence of increasing amounts of the FLAG-RanBPM expression plasmid (25, 50, or 100 ng). At 48 h after transfection, cells were lysed and their luciferase activities were measured. Firefly luminescence signal was normalized based on the *Renilla* luminescence signal. (**b**) RanBPM stimulates the p73α-mediated growth suppression. H1299 cells were co-transfected with the indicated combinations of the expression plasmid together with the constant amount of the expression plasmid for β-galactosidase (125 ng) (pCH110, Amersham Pharmacia Biotech). At 48 h after transfection, transfected cells were identified by staining with 5-bromo-4-chloro-3-indolyl-β-D-galactopyranoside (X-gal). The relative percentage of β-gal-positive cells represents the ratio of the number of β-gal-positive cells to that of those transfected with pcDNA3 alone. (**c**) Colony formation assay. H1299 cells were transfected with HA-p73α (200 ng), FLAG-RanBPM (750 ng) or HA-p73α (200 ng) plus FLAG-RanBPM (750 ng). Total amount of plasmid DNA was kept constant (1 μg) with pcDNA3, and pcDNA3 alone was used as a negative control. At 2 days after transfection, cells were selected with G418 (400 μg/ml) for 2 weeks. G418-resistant colonies were fixed in methanol, and stained with Giemsa's solution. Representative dishes of three independent experiments are shown. (**d**) RanBPM enhances the p73α-mediated apoptosis. H1299 cells transfected with 0.2 μg of the GFP expression plasmid and 0.5 μg of the HA-p73α expression plasmid together with or without 1.5 μg of the FLAG-RanBPM expression plasmid. At 48 h after transfection, transfected cells were identified by the presence of green fluorescence. Cell nucleus was stained with DAPI to reveal nuclear condensation and fragmentation. The number of GFP-positive cells with apoptotic nuclei was scored

restores its function, indicating that p73α displaces p53 from the cytoplasmic complex containing Parc. It is thus likely that p73α could modulate cellular proteins/pathways that specifically regulate nuclear import and export of RanBPM. Since RanBPM is associated with a variety of nuclear proteins, p73α might play a critical role in regulating nuclear function of RanBPM.

Acknowledgements
We are grateful to Dr S Sakiyama for helpful discussion. This work was supported in part by a Grant-in-Aid from the Ministry of Health and Welfare for a New 10-Year Strategy for Cancer Control, a Grant-in-Aid for Scientific Research on Priority Areas, a Grant-in-Aid for Scientific Research (B) from the Ministry of Education, Science, Sports and Culture, Japan, and a found from the Hisamitsu Pharmaceutical Company.

References

Agami R, Blandino G, Oren M and Shaul Y. (1999). *Nature*, **399,** 809–813.
Bai D, Chen H and Huang BR. (2003). *Biochem. Biophys. Res. Commun.*, **309,** 552–557.
Balint E, Bates S and Vousden KH. (1999). *Oncogene*, **18,** 3923–3929.
Carrano AC, Eytan E, Hershko A and Pagano M. (1999). *Nat. Cell Biol.*, **1,** 193–199.
Di Como CJ, Gaiddon C and Prives C. (1999). *Mol. Cell. Biol.*, **19,** 1438–1449.
Ganoth D, Bornstein G, Ko TK, Larsen B, Tyers M, Pagano M and Hershko A. (2001). *Nat. Cell Biol.*, **3,** 321–324.
Goldschneider D, Blanc E, Raguenez G, Barrois M, Legrand A, Le Roux G, Haddada H, Bebard J and Douc-Rasy S. (2004). *J. Cell Sci.*, **117,** 293–301.
Gong J, Costanzo A, Yang H-Q, Melino G, Kaelin WG, Levrero M and Wang JYJ. (1999). *Nature*, **399,** 806–809.
Ideguchi H, Ueda A, Tanaka M, Yang J, Tsuji T, Ohno S, Hagiwara E, Aoki A and Ishigatsubo Y. (2002). *Biochem. J.*, **367,** 87–95.
Jost C, Marin M and Kaelin WG. (1997). *Nature*, **389,** 191–194.
Kaghad M, Bonnet H, Yang A, Creancier L, Biscan JC, Valent A, Minty A, Chalon P, Lelias JM, Dumont X, Ferrara P, McKeon F and Caput D. (1997). *Cell*, **90,** 809–819.
Lee C-W and La Thangue NB. (1999). *Oncogene*, **18,** 4171–4181.
Li M, Chen D, Shiloh A, Luo J, Nikolaev AY, Qin J and Gu W. (2002). *Nature*, **416,** 648–653.
Lutz W, Frank EM, Craig TA, Thompson R, Venters RA, Kojetin D, Cavanagh J and Kumar R. (2003). *Biochem. Biophys. Res. Commun.*, **303,** 1186–1192.
Melino G, De Laurenzi V and Vousden KH. (2002). *Nat. Rev. Cancer*, **2,** 605–615.
Moll UM, Ostermeyer AG, Haladay R, Winkfield B, Frazier M and Zambetti G. (1996). *Mol. Cell. Biol.*, **16,** 1126–1137.
Nakagawa T, Takahashi M, Ozaki T, Watanabe K, Todo S, Mizuguchi H, Hayakawa T and Nakagawara A. (2002). *Mol. Cell. Biol.*, **22,** 2575–2585.
Nakamura M, Masuda H, Horii J, Kuma K, Yokoyama N, Ohba T, Nishitani H, Miyata T, Tanaka M and Nishimoto T. (1998). *J. Cell Biol.*, **143,** 1041–1052.
Nikolaev AY, Li M, Puskas N, Qin J and Gu W. (2003). *Cell*, **112,** 29–40.
Nishitani H, Hirose E, Uchimura Y, Nakamura N, Umeda M, Nishii K, Mori N and Nishimoto T. (2001). *Gene*, **272,** 25–33.
Ohtsuka T, Ryu H, Minamishima YA, Ryo A and Lee SW. (2003). *Oncogene*, **22,** 1678–1687.
Ozaki T, Watanabe K, Nakagawa T, Miyazaki K, Takahashi M and Nakagawara A. (2003). *Oncogene*, **22,** 3231–3242.
Ponting C, Schultz J and Bork P. (1997). *Trends Biochem. Sci.*, **22,** 193–194.
Pozniak CD, Radinovic S, Yang A, McKeon F, Kaplan DR and Miller FD. (2000). *Science*, **289,** 304–306.
Rao MA, Cheng H, Quayle AN, Nishitani H, Nelson CC and Rennie PS. (2002). *J. Biol. Chem.*, **277,** 48020–48027.
Ren J, Datta R, Shioya H, Li Y, Oki E, Biedermann V, Bharti A and Kufe D. (2002). *J. Biol. Chem.*, **277,** 33758–33765.
Stiewe T, Zimmermann S, Frilling A, Esche H and Putzer BM. (2002). *Cancer Res.*, **62,** 3598–3602.
Umeda M, Nishitani H and Nishimoto T. (2003). *Gene*, **303,** 47–54.
Wang D, Li Z, Messing EM and Wu G. (2002). *J. Biol. Chem.*, **277,** 36216–36222.
Wang Y, Schneider M, Li X, Duttenhofer I, Debatin K-M and Hug H. (2002). *Biochem. Biophys. Res. Commun.*, **297,** 148–153.
Watanabe K, Ozaki T, Nakagawa T, Miyazaki K, Takahashi M, Hosoda M, Hayashi S, Todo S and Nakagawara A. (2002). *J. Biol. Chem.*, **277,** 15113–15123.
Yuan Z-M, Shioya H, Ishiko T, Sun X, Gu J, Huang YY, Lu H, Kharbanda S, Weichselbaum R and Kufe D. (1999). *Nature*, **399,** 814–817.
Zeng X, Chen L, Jost CA, Maya R, Keller D, Wang X, Kaelin WG, Oren M, Chen J and Lu H. (1999). *Mol. Cell. Biol.*, **19,** 3257–3266.

Differentially expressed genes throughout the cellular immortalization processes are quite different between normal human fibroblasts and endothelial cells

KEIKO HIYAMA[1], KEIKO OTANI[2,3], MEGU OHTAKI[2], KENICHI SATOH[2], TSUTOMU KUMAZAKI[1,4], TOMOKO TAKAHASHI[5], YOUJI MITSUI[5], YASUSHI OKAZAKI[6], YOSHIHIDE HAYASHIZAKI[6], HIDEAKI OMATSU[1,7], TAKUYA NOGUCHI[1], KEIJI TANIMOTO[1] and MASAHIKO NISHIYAMA[1]

Departments of [1]Translational Cancer Research, [2]Environmetrics and Biometrics, Research Institute for Radiation Biology and Medicine (RIRBM), Hiroshima University, Hiroshima 734-8553; [3]Japan Biological Informatics Consortium; [4]Suzugamine Women's College, Hiroshima; [5]Department of Pharmaceutical Technology, Faculty of Pharmaceutical Science at Kagawa Campus, Tokushima Bunri University, Kagawa; [6]Laboratory for Genome Exploration Research Group, Riken Genomic Sciences Center (GSC), Riken Yokohama Institute, Yokohama; [7]Department of Hospital Pharmacy, School of Medicine, Kobe University, Kobe, Japan

Received January 17, 2005; Accepted March 4, 2005

Abstract. It is widely accepted that activation of telomerase and maintenance of telomeres play central roles in cellular immortalization for most cancer cells. However, they seem to be insufficient for normal human cells. To elucidate critically responsible genes for telomerase mediated cellular immortalization in non-cancerous cells, we explored the genes that are differentially expressed throughout the immortalization process of normal human cells using cDNA microarrays with novel normalization procedures. We found that the number of genes, differentially expressed during cellular immortalization after ectopic expression of telomerase, dramatically increased in a later phase, especially in fibroblasts. We identified 18 and 20 genes/ESTs dysregulated throughout the cellular immortalization processes in fibroblasts and endothelial cells, respectively, but none of them overlapped. Only *BGN* and *COL5A2* were commonly downregulated, except for at early phase in fibroblasts, and a few genes showed controversial expression changes, with regard to previous reports in cancer cells. These findings indicate that normal somatic cells would require cell-type specific events in addition to telomerase activation, and a rare population that eventually experience such events would acquire immortality. The key molecules that distinguish the immortalization mechanisms in cancerous and non-cancerous cells may become crucial targets for anticancer therapy and regenerative therapy.

Correspondence to: Dr Keiko Hiyama, Department of Translational Cancer Research, Research Institute for Radiation Biology and Medicine, Hiroshima University, 1-2-3 Kasumi, Minami-ku, Hiroshima 734-8553, Japan
E-mail: khiyama@hiroshima-u.ac.jp

Key words: telomerase, immortalization, cDNA microarray, mixed normal distribution, normalization

Introduction

Telomere and telomerase, which govern cellular life span, have been intensively studied since the re-evaluation of the historical hypothesis of 'endreplication problem' (1) on the 'Hayflick limit' (2) of normal cells and the discovery of telomerase in Tetrahymena (3). When the 'telomere hypothesis' (4) was proposed and supported by subsequent experimental evidence (5), most researchers believed that the mysterious story of the end of chromosomes was forming a satisfactory conclusion. However, several unexpected aspects were unveiled, which deviated from the original 'telomere hypothesis' that telomerase activation occurs at or near crisis (4). We had shown that human normal lymphocytes and hematopoietic stem/progenitor cells have innate telomerase activity that can be upregulated upon stimulation of proliferation (6) as in other self-renewal tissues such as intestinal cripts (7), hair follicles (8), and endometrium (9), while considerable parts of clinically malignant neoplasms still contain 'mortal' cancer cells without telomerase activity (10-12). Several reports inferred the differences in the capacity of telomerase in cellular immortalization between normal somatic cells and cancer cells: upregulation of telomerase during T cell activation is transient and does not prevent the loss of telomeres in long-term cultures (13), while it is maintained even after long-term culture in cancer cell lines (5). Transient expression of telomerase through S phase was found in normal fibroblasts (14), whereas telomerase activity in immortal cancer cell lines is known not to change during progression through the stages of cell cycle (15). Even among non-cancerous cells, some normal human cells can be immortalized concomitant with ectopic expression of telomerase (16,17), while others cannot, under any condition,

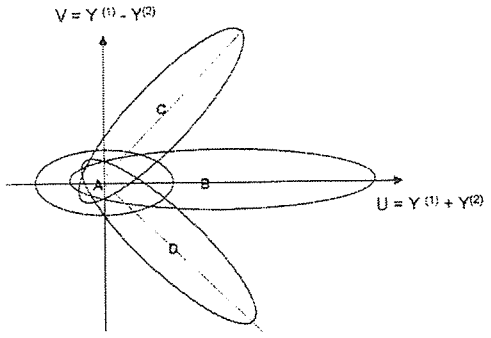

Figure 1. The two-dimensional mixed normal model with four components for S-D plot proposed by Ohtaki *et al* (23) is shown schematically. The x-axis indicates the sum of expression intensities of the query and reference samples and the y-axis indicates the difference of them. The status of genes inside the regions A, B, C, and D are (off, off), (on, on), (on, off), and (off, on) in the query and reference samples, respectively.

even maintain telomere length by telomerase (18). In mouse, it was also reported that mouse telomerase, mTERT, would play a role in suppressing the transformation phenotype.

Such findings lead us to the idea that the mechanisms of cellular immortalization through activation of telomerase are different among the non-cancerous cells and between cancerous and non-cancerous cells. We previously investigated the chronological changes in the expression levels of the cell-cycle/apoptosis related genes by real-time RT-PCR in human normal fibroblasts and endothelial cells transfected with *hTERT*, the human telomerase reverse transcriptase gene. We found that human foreskin fibroblast MJ90 cells required intrinsic responses including reversible up-regulation of cell-cycle promoting genes and downregulation of apoptosis-inducing genes in early phase after transfection, whereas the HUE142-2 endothelial cells did not (19). In addition, the microarray analysis of the immortalized fibroblasts at PDL 216 revealed that their dysregulated genes were different from those previously reported in BJ cells, another kind of foreskin fibroblast (20).

However, the snapshot analysis of expression profiles during cellular immortalization using microarray technique may mislead us to junk genes that would be temporally dysregulated with many other genes. To elucidate the critically responsible genes for cellular immortalization, we focused the genes that are differentially expressed throughout the immortalization process in these cells using cDNA microarrays. Microarray technology is one of the most effective high-throughput tools at present that facilitates the identification of specific genes among tens of thousands of background genes (21), but several serious problems have been pointed out that are to be overcome before finding the genuine target (22). One of the critical problems is the procession of a large amount of data. In cDNA microarray experiments, differentially expressed genes between a query and a reference sample are identified through many processes using two different fluorescent dyes. There could be large systematic variations that affect the resultant estimated gene expression levels. To accomplish our purpose to explore the truly differentially expressed genes during cellular immortalization, we applied the novel statistical procedure proposed by Ohtaki *et al* (23) that removes the systematic variations from the obtained cDNA microarray gene expression data and estimates the probability of the genes differently expressed between the two cell types, with the concept illustrated in Fig. 1.

Materials and methods

Cell culture and transfection of hTERT. Cell culture and *hTERT* transfection were carried out as previously described (19). Briefly, a normal neonatal human diploid fibroblast strain MJ90 was cultured in Dulbecco's modified Eagle's minimal essential medium (DMEM; Sigma-Aldrich Japan, Tokyo, Japan) supplemented with 2 mM L-glutamine (Life Technologies, Rockville, MD, USA) and 10% fetal calf serum (FCS; Life Technologies). A normal human umbilical vein endothelial cell strain HUE142-2 was grown in MCDB151 medium (Sigma-Aldrich Japan) supplemented with 15% fetal bovine serum, 5 μg/ml of heparin (Sigma), and 5 ng/ml of recombinant acidic fibroblast growth factor in a plastic flask (Corning) precoated with bovine fibronectin solution (1 μg/cm^2, Wako, Osaka, Japan).

The *hTERT* expression plasmids hTRT/FLAG and hTERTn2 (24) were kindly provided by Professor F. Ishikawa (Kyoto University, Kyoto, Japan). The 40 μg of plasmid hTRT/FLAG or hTERTn2 linealized by a single cut with a restriction enzyme *Nru*I was transfected into 10^7 MJ90 cells at PDL (population doubling level) 41 or the HUE142-2 cells at PDL 35 by electroporation (Invitrogen, San Diego, CA, USA) at 330 V (19). Clones harboring the plasmids were obtained by 400 μg/ml of G418 selection (Wako) and named as TF1 from MJ90 and nTE4-5 from the HUE142-2 cells. The TF1 cells at PDL 104, 148, and 216 and nTE4-5 cells at PDL 105, 145, and 216 were collected and stored at -80˚C until use. Expression of *hTERT* mRNA and telomerase activity in TF1 and nTE4-5 cells and absence of them in MJ90 and HUE142-2 cells had been previously confirmed by real-time RT-PCR and telomeric repeat amplification Protocol (TRAP) assay (19).

Preparation of RNA. Total RNA was extracted from the cultured cells using an RNeasy™ total RNA isolation kit (Qiagen, Hilden, Germany) according to the protocols the manufacturer recommended. The poly(A)-RNA was isolated from the extracted total RNA using μMACS™ mRNA isolation kit (Miltenyi Biotec, Bergisch Gladbach, Germany).

Microarray analysis. One-μg poly(A)-RNA samples extracted from cell strains after hTERT induction were labeled with the fluorescent dye Cy-3 by random-primed reverse transcription. Similarly, 1-μg poly(A)-RNA samples extracted from MJ90 cells at PDL 30 and the HUE142-2 cells at PDL 38 before *hTERT* induction were labeled with Cy-5, and used as the expression references for TF1 and nTE4-5 strains, respectively. Each pair of Cy-3 and Cy-5 labeled cDNAs were hybridized as probes on RIKEN human 21K arrays as previously described (25). The array contained 21,168 spots in 48 blocks (4x12), each containing 441 spots (21x21). Among them, 20,784 spots are human cDNA clones purchased from ResGen™ (Invitrogen Corporation, Carlsbad, CA, USA) and the remaining spots are

the internal and exogenous controls spotted on every subgrid as positive and negative controls. Each spot was numbered from 1 to 21,168 as gene ID, and a coordinate axis was introduced in each sub grid. All microarray analyses on the six pairs, i.e. MJ90 vs. TF1-PDL 104, TF1-PDL 148, or TF1-PDL 216 and HUE142-2 vs. nTE4-5-PDL 105, nTE4-5-PDL 145, or nTE4-5-PDL 216 were carried out in duplicate.

Data collection. Arrays were laser-scanned using ScanArray 5000 confocal laser scanner (GSI Lumonics), and the fluorescence measurements were made separately by channels 1 and 2 for each dye at each spot on the array. Let CH1I and CH2I be spot intensities scanned by channels 1 and 2, respectively. Let CH1B and CH2B be their background intensities. In this study, the value of CH1 = CH1I - CH1B and CH2 = CH2I - CH2B were used as a gene expression level in each sample. The microarray data are available at the Gene Expression Omnibus, http://www.ncbi.nlm.nih.gov/geo/, under GEO accession no. GSE1900. Each result of the duplicated microarray experiment was normalized independently as described below and then the average of these 2 normalized data on each spot was subjected to the proposed normalization again, to obtain the final value.

Statistical method. Ohtaki *et al* proposed a mathematical model based on the functional status of the genes to remove the systematic errors in the microarray data and identify differentially expressed genes between the two cell types (23). Briefly, the following explanation was given for an individual observed measurement. An observed measurement for each channel consists of a true signal with fluctuation, a systematic error common to channels 1 and 2, and a measurement error independent between the two channels. As sources of systematic error, labeling efficiencies of the differing dyes, different scanning properties, and spatial location effects on spot are considered. Reduction of systemic errors is referred to as 'normalization'. The terms 'on' and 'off' are used to express the functional status of a gene. If a gene is really expressed yielding its product (i.e. 'mRNA') as the true signal, they call the status 'on', otherwise, (i.e., mRNA is not in the sample), they call it 'off'. When the status of a gene is 'off', the observed measurement reflects only the amount of systematic error and measurement error.

The mathematical model for the microarray data with each channel (denoted as $Y_i^{(1)}$ and $Y_i^{(2)}$, where $Y_i^{(1)}$ and $Y_i^{(2)}$ are the suitably transformed and normalized gene expression measurements) is described as:

$$\begin{cases} Y_i^{(1)} = \tau_i^{(1)}\alpha_i + \beta_i + \varepsilon_i^{(1)}, \\ Y_i^{(2)} = \tau_i^{(2)}\alpha_i + \beta_i + \varepsilon_i^{(2)}. \end{cases}$$

The symbols $\tau_i^{(1)}$ and $\tau_i^{(2)}$ represent the expression status of gene i in the query and reference samples (if gene i is 'on', $\tau_i = 1$; if gene i is 'off', $\tau_i = 0$). The symbol α_i represents the expression intensity of gene i when it is 'on'. The symbol β_i denotes systematic error common to channels 1 and 2. The symbols $\varepsilon_i^{(1)}$ and $\varepsilon_i^{(2)}$ indicate random errors, which are mutually independent. They introduced the variable transformation $U = Y_i^{(1)} + Y_i^{(2)}$ and $V = Y_i^{(1)} - Y_i^{(2)}$. The gene was characterized by the joint sum and difference of its expression intensities in two samples. They called the plot (U,V) as the S-D plot. Then they applied a two-dimensional mixed normal model with four components. Fig. 1 illustrates the concepts of the model. The genes of interest to us belong to the regions C ('on', 'off') and D ('off', 'on'), where V reflects the true difference of expression intensities between the two samples. On the contrary, genes belonging to the regions A and B (Fig. 1) are not informative, because V reflects only the measurement error. The probability of the gene being differentially expressed between the query and the reference samples, i.e., the status of the gene being between 'on', 'off' and 'off', 'on', was obtained as a posterior probability.

Real-time RT-PCR. For representative genes detected by microarray analysis as differentially expressed between the cell lines before and after *hTERT* transfection, or as showing discrepancies between global normalization and the proposed normalization, quantitative real-time RT-PCR analysis was carried out. Two-μg total RNA extracted from each cell line was reverse-transcribed using a High-Capacity cDNA Archive™ Kit (Applied Biosystems, CA, USA), and one-hundredth aliquot was subjected to real-time RT-PCR using Assays-on-Demand™ gene expression products or pre-developed TaqMan™ assay reagents with ABI PRISM 7700 or 7900 sequence detection systems (PE Applied Biosystems), as previously described (19). The mRNA expression level was evaluated by the ratio = (value of target gene)/(value of *GAPD* or *ACTB*), and this value of each *hTERT* transfected strain was divided by that of the parent strain. Every reaction was carried out in triplicate.

Results

Cell culture and transfection of hTERT. After the transfection of the *hTERT*-expressing hTRT/FLAG plasmid into the fibroblasts MJ90 at PDL 41, 7 clones with telomerase expression were isolated but fell into apoptosis before they reached PDL 90 except for one clone, TF1. TF1 was sequentially cultured until PDL 216 and considered to be immortal.

For endothelial cells, we first tried to use the hTRT/FLAG plasmid twice but no clone was obtained. Then we transfected another *hTERT*-expressing plasmid, hTERTn2, into HUE142-2 cells at PDL 35 and obtained 2 clones with positive telomerase expression. One of these clones, nTE4-5, continued to proliferate over PDL 216 and was considered to be immortal, but another clone fell into apoptosis quickly. The growth curve of the TF1 strain revealed to be slow until ~PDL 120 where it turned to rapid growth, while it was straight and rapid from just after the *hTERT* transfection in the nTE4-5 cells (19).

Microarray analysis. After removing the predictable systematic errors by using proposed normalization (23), the difference of the relative expression levels of each gene between the *hTERT* transfected cells and the control parent cells was given as the difference of their spot intensities. To confirm the feasibility of the proposed normalization, the processed signal intensities of the *GAPD* gene, a housekeeping gene encoding glyceraldehyde-3-phosphate dehydrogenase, spotted in every subgrid, were compared to those with global

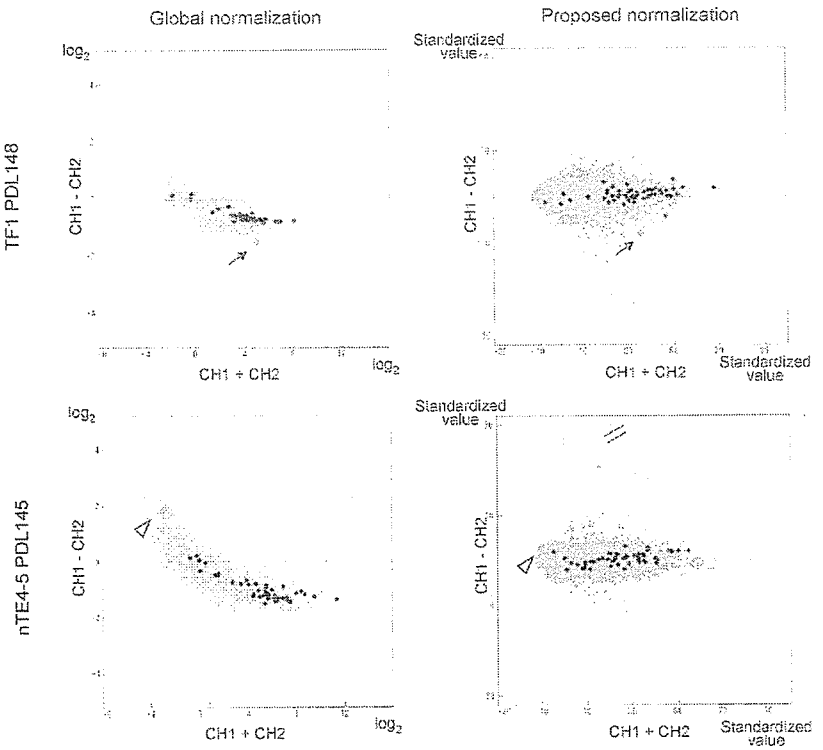

Figure 2. S-D plots of cDNA microarray data in representative 2 cell strains with global normalization (left) and proposed normalization (right). Upper, TF1 at PDL 148 (CH1, Cy3) compared with MJ90 (CH2, Cy5); lower, nTE4-5 at PDL 145 (CH1, Cy3) compared with HUE142-2 (CH2, Cy5); large black dots, 51 *GAPD*, a housekeeping gene, spots located in every subgrid; large pink dots with arrows (upper), *ALDH1A1*; large pink dots with open arrow heads (lower), *EREG*; gray dots (left), all remaining spots with global normalization. Each color of the dots in right represents the probability of the gene to be differentially expressed between the *hTERT* transfected cells and the control parent cells as 0.8< red ≤1.0, 0.6< yellow ≤0.8, 0.4< lime ≤0.6, 0.2< aqua ≤0.4, and 0≤ blue ≤0.2, respectively.

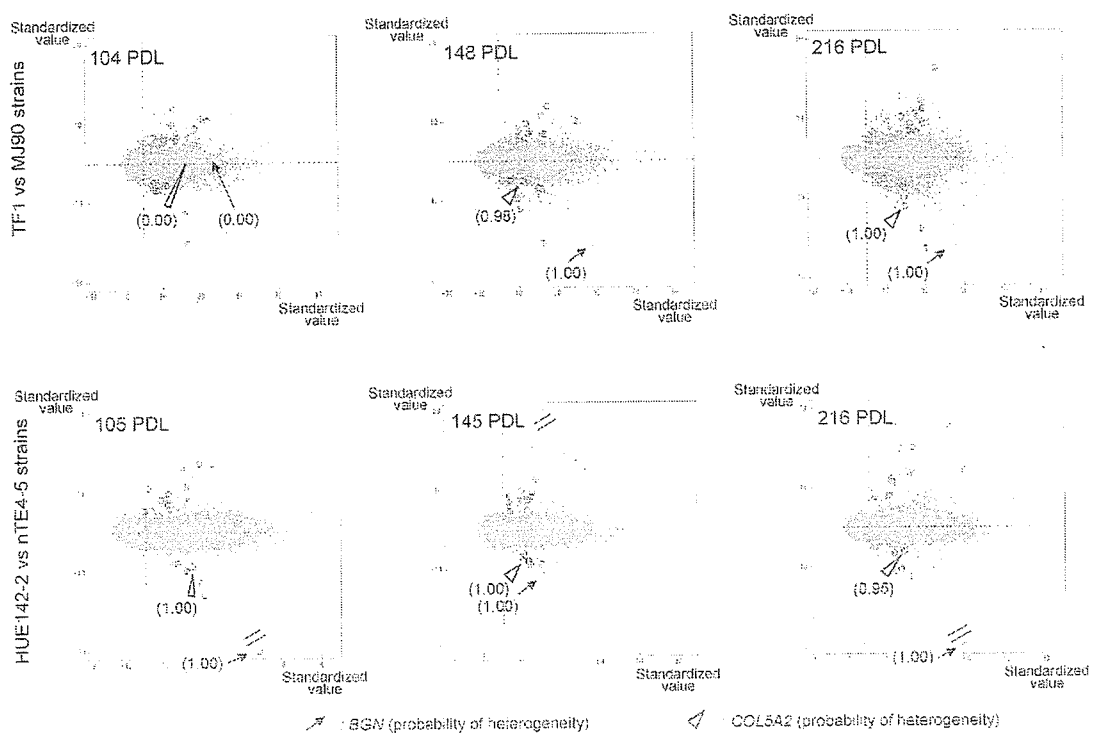

Figure 3. S-D plots of cDNA microarray data with proposed normalization showing chronological changes after *hTERT*-transfection in fibroblasts (upper) and endothelial cells (lower). Each color of the dots represents the probability of the gene to be differentially expressed between the *hTERT*-transfected cells and the control parent cells as 0.8< red ≤1.0, 0.6< yellow ≤0.8, 0.4< lime ≤0.6, 0.2< aqua ≤0.4, and 0≤ blue ≤0.2, respectively. Open circles, the genes differentially expressed with the probability of heterogeneity ≥0.5 commonly in TF1 strains or nTE4-5 strains; arrows, *BGN*; open arrow heads, *COL5A2*.

Table I. Number of clones differentially expressed with probability ≥0.5 during cellular immortalization in normal human fibroblasts (TF1) and endothelial cells (nTE4-5).

	PDL		
TF1	104	148	216
Upregulated	108	87	357
Downregulated	55	182	337
Total	163	269	694

	PDL		
nTE4-5	105	145	216
Upregulated	69	61	123
Downregulated	29	21	102
Total	98	82	225

normalization. Fig. 2 shows the S-D plots of representative cell strains, TF1 cells at PDL 148 as CH1 and MJ90 cells as CH2 (upper), and nTE4-5 cells at PDL 145 as CH1 and HUE142-2 cells as CH2 (lower), with global normalization (left) and the proposed normalization (right). For global normalization, each value in y-axis was calculated with the following formula: $Y = \log_2 [\{(Cy3 \text{ row signal}) - (Cy3 \text{ background})\}/\text{median}] - \log_2 [\{(Cy5 \text{ row signal}) - (Cy5 \text{ background})\}/\text{median}]$. By the proposed normalization, the distortion observed in the global normalization was corrected, and all *GAPD* spots concentrated around the baseline. The representative genes *ALDH1A1* in TF1 cells at PDL 148 (Fig. 2, large pink dots with arrows, upper) and *EREG* in nTE4-5 cells at PDL 145 (Fig. 2, large pink dots with open arrow heads, lower) showing as differentially expressed in global normalization came to be classified as comparably expressed 'on, on' or 'off, off', respectively, with low probability of heterogeneity with the proposed normalization.

The S-D plots of the whole 21,168 clones comparing the cells before and after the *hTERT* transfection at each PDL are shown in Fig. 3. The open circles represent the continuously upregulated or downregulated genes after *hTERT* transfection at any PDL in fibroblast strains or endothelial strains with the probability of heterogeneity ≥0.5.

The number of genes differentially expressed with probability ≥0.5 between the *hTERT* transfected cells (TF1 and nTE4-5 strains) at each PDL and the corresponding parent cells (MJ90 and HUE142-2 strains) are listed in Table I. Among them, 10 genes (*SOD3, LGALS3BP, FABP3, RAGE, ABCA1, EPAS1, AKR1C3, EPHX1, PRNP*, and *DPP7*) were continuously upregulated throughout the immortalization process of fibroblast strains, at 104, 148, and 216 PDLs. On the contrary, 7 genes (*MMP3, C18orf4, GOPC, TNC, DOK5, MATN2*, and *KRTHA4*) and an EST were commonly downregulated (Table II). For endothelial cells, 10 genes (*UNC13D, T1A-2, KRT7, PSG4, HOP, PSG5, PSG3, C17orf31, FST*, and *PSG1*) and 3 ESTs were found to be continuously upregulated through the immortalization process at 105, 145, and 216 PDLs, and 5 genes (*BGN, ERBB2, ACP5, KIAA0746*, and *COL5A2*) and 2 ESTS as continuously repressed. Nevertheless, there were no overlapped genes that were dysregulated throughout the immortalization processes in both fibroblasts and endothelial cells, and furthermore, a few genes showed controversial expression changes with previous reports in cancer cells. Only *BGN* and *COL5A2* were commonly downregulated, except for at early phase in fibroblasts (Fig. 3).

Real-time RT-PCR. For the representative genes demonstrating differential expression in immortal cells or those with contradictory results between global normalization and the proposed normalization, mRNA expression level in each cell strain was estimated by real-time RT-PCR for comparison. Fig. 4 shows the mean values of the comparative expression levels of the representative genes evaluated by real-time RT-PCR (adjusted with *GAPD* and *ACTB*) and cDNA microarray with global normalization, and the probability of heterogeneity calculated by the proposed normalization. The probability of heterogeneity was minimum in general for the spots that showed controversial expression changes between real-time RT-PCR and cDNA microarray with global normalization, or among the real-time RT-PCR data adjusted with *GAPD* or *ACTB*.

Discussion

We found that genes differentially expressed during cellular immortalization after *hTERT* transfection were dramatically increased in later phase especially in fibroblasts, and the number of the dysregulated genes was larger in fibroblasts than in endothelial cells (Table I). We previously found that telomere length (TRF length) in HUE142-2 was 8.0 kb and was stably maintained after *hTERT* transfection, while those in fibroblasts were once shortened even with telomerase expression and recovered at 216 PDL: 8.1, 6.1, 6.8, and 8.4 kb for MJ90, TF1-PDL 104, 148, and 216 cells, respectively (19). Furthermore, the upregulation of anti-apoptotic genes and downregulation of pro-apoptotic or apoptosis-related genes were demonstrated in the TF1 cells, especially in early phase after *hTERT* transfection where telomere-maintenance mechanism had not been completed, while such findings were not observed in the nTE4-5 cells. These findings suggest that turning from telomerase-positive slow-growing cells without telomere-maintenance mechanism to rapid and continuously growing cells with telomere-maintenance mechanism may require some intrinsic events in cell-type specific manner, possibly more in fibroblast MJ90 than in endothelial cell HUE142-2.

Although some of the differentially expressed genes at early phase could be influenced nonspecifically by gene transfection, genes being dysregulated later might not be, including the genes truly responsible for the intrinsic secondary events required for cellular immortalization. A chronological analysis using microarray is likely to be the best method of identification because we could insure the reproducibility of the data. This study demonstrated that our proposed normalization could correct the distortion of the array data possibly caused by the difference of sensitivity of Cy3 and Cy5, and avoid the large part of false positive result

Table II. Differentially expressed genes continuously through the cellular immortalization in normal human fibroblasts (TF1) and endothelial cells (nTE4-5).

Gene	CH1-CH2 (probability of heterogeneity) 104 PDL	148 PDL	216 PDL
Upregulated in TF1			
Superoxide dismutase 3, extracellular (*SOD3*)	13.78 (1.00)	11.54 (1.00)	11.73 (1.00)
Lectin, galactoside-binding, soluble, 3 binding protein (*LGALS3BP*)	9.81 (1.00)	13.76 (1.00)	22.51 (1.00)
Fatty acid binding protein 3 (*FABP3*)	6.68 (1.00)	9.35 (1.00)	10.44 (1.00)
Renal tumor antigen (*RAGE*)	6.28 (1.00)	7.58 (1.00)	8.82 (1.00)
ATP-binding cassette, sub-family A, member 1 (*ABCA1*)	6.68 (1.00)	6.35 (1.00)	6.53 (0.99)
Endothelial PAS domain protein 1 (*EPAS1*)	7.70 (1.00)	5.82 (0.95)	6.95 (1.00)
Aldo-keto reductase family 1, member C3 (*AKR1C3*)	10.86 (1.00)	10.02 (0.75)	6.514 (0.78)
Epoxide hydrolase 1, microsomal (*EPHX1*)	8.97 (1.00)	6.71 (0.54)	12.41 (1.00)
Prion protein (*PRNP*)	5.68 (0.68)	6.85 (1.00)	14.55 (1.00)
Dipeptidyl peptidase II (*QPP*; *DPP7*)	6.73 (0.59)	6.87 (0.84)	8.75 (1.00)
Downregulated in TF1			
Matrix metalloproteinase 3 (*MMP3*)	-20.19 (1.00)	-20.89 (1.00)	-22.71 (1.00)
Homo sapiens cDNA FLJ11477 fis, clone HEMBA1001746 (*C18orf4*)	-6.74 (1.00)	-7.77 (1.00)	-8.67 (1.00)
Homo sapiens cDNA: FLJ21421 fis, clone COL04123 (*GOPC*)	-6.32 (1.00)	-7.77 (1.00)	-8.67 (1.00)
Hexabrachion (tenascin C) (*TNC*; *HXB*)	-12.61 (1.00)	-7.11 (0.98)	-17.64 (1.00)
Hypothetical protein (LOC55816; *C20orf180*; *DOK5*)	-6.49 (0.99)	-8.51 (1.00)	-6.28 (0.99)
Matrilin 2 (*MATN2*)	-5.60 (0.89)	-9.42 (1.00)	-9.88 (1.00)
EST (W52341 l AA284245)	-5.45 (0.88)	-5.12 (0.86)	-7.19 (1.00)
Keratin, hair, acidic, 4 (*KRTHA4*)	-4.76 (0.66)	-4.92 (0.90)	-5.30 (0.99)

Gene	CH1-CH2 (probability of heterogeneity) 105 PDL	145 PDL	216 PDL
Upregulated in nTE4-5			
Homo sapiens mRNA for FLJ00067 protein (*UNC13D*)	17.30 (1.00)	8.44 (1.00)	20.39 (1.00)
Lung type-I cell membrane-associated glycoprotein (*T1A-2*)	16.02 (1.00)	18.14 (1.00)	25.64 (1.00)
Keratin 7 (*KRT7*)	15.87 (1.00)	14.56 (1.00)	14.43 (1.00)
Pregnancy specific ß-1-glycoprotein 4 (*PSG4*)	15.77 (1.00)	12.79 (1.00)	19.99 (1.00)
EST (AA504137; *HOP*)	12.53 (1.00)	9.56 (1.00)	13.41 (1.00)
EST (W51985; *PSG5*)	10.97 (1.00)	8.14 (1.00)	14.67 (1.00)
EST (W60894)	8.73 (1.00)	8.42 (1.00)	13.67 (1.00)
Pregnancy specific ß-1-glycoprotein 3 (*PSG3*)	8.68 (1.00)	9.95 (1.00)	12.36 (1.00)
KIAA0732 protein (*C17orf31*)	8.30 (1.00)	7.43 (1.00)	7.89 (1.00)
Follistatin (*FST*)	6.99 (1.00)	7.61 (1.00)	11.15 (1.00)
EST (H86461)	9.69 (1.00)	4.84 (0.56)	11.52 (1.00)
Pregnancy specific ß-1-glycoprotein 1 (*PSG1*)	11.07 (0.99)	7.09 (1.00)	19.73 (1.00)
EST (R73909)	5.32 (0.51)	8.62 (1.00)	7.53 (0.99)
Downregulated in nTE4-5			
Biglycan (*BGN*)	-31.13 (1.00)	-11.44 (1.00)	-33.93 (1.00)
Homo sapiens clone IMAGE:110582 mRNA	-12.71 (1.00)	-8.65 (1.00)	-12.46 (1.00)
v-erb-b2 avian erythroblastic leukemia viral oncogene homolog 2 (*ERBB2*)	-9.534 (1.00)	-8.57 (1.00)	-11.04 (1.00)
Acid phosphatase 5, tartrate resistant (ACP5)	-15.82 (1.00)	-7.67 (1.00)	-10.33 (1.00)
KIAA0746 protein (*KIAA0746*)	-7.74 (1.00)	-6.72 (1.00)	-10.57 (1.00)
Collagen, type V, α 2 (*COL5A2*)	-8.46 (1.00)	-7.73 (1.00)	-6.09 (0.95)
EST (N45282)	-8.11 (1.00)	-5.87 (0.92)	-6.57 (1.00)

CH1: TF1 or nTE4-5; CH2: MJ90 or HUE142-2. Heterogeneity: ('on', 'off') or ('off', 'on').

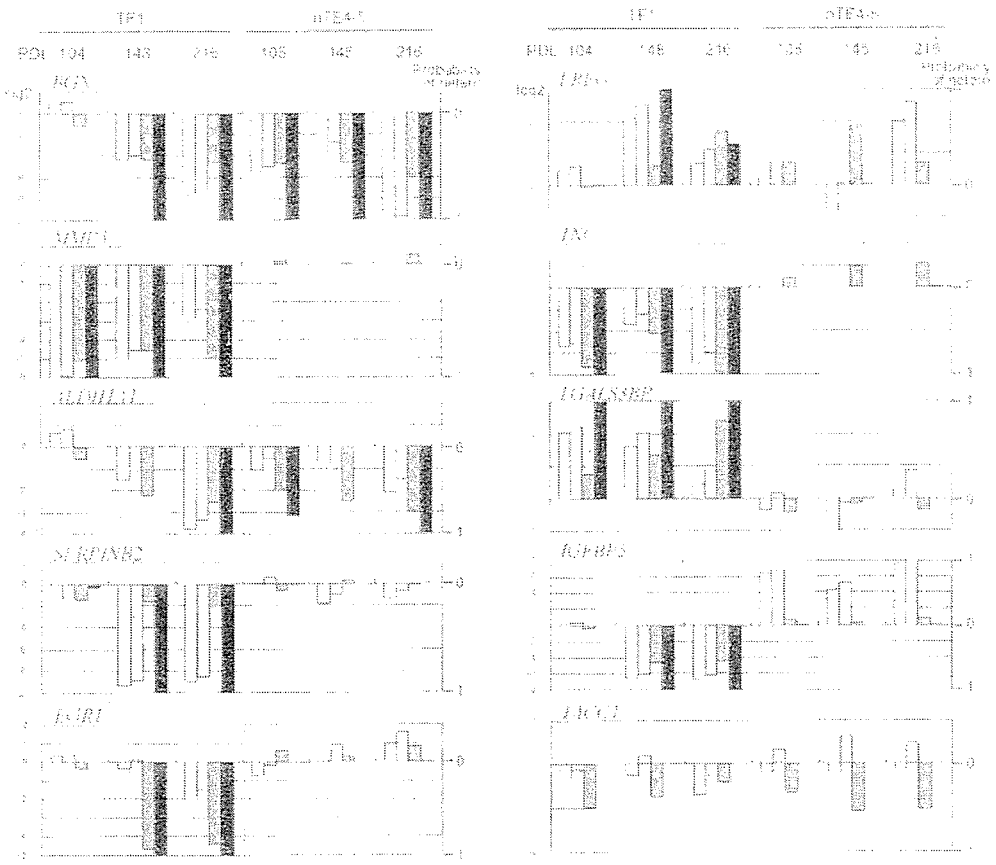

Figure 4. Changes in expression levels from corresponding parent cells are compared between real-time RT-PCR and cDNA microarray data with global normalization and probability of heterogeneity calculated by the proposed normalization for representative genes. Open bar, real-time RT-PCR adjusted with GAPD (left scale); dotted bar, real-time RT-PCR adjusted with *ACTB* (left scale); hatched bar, cDNA microarray with global normalization (left scale); black bar, cDNA microarray with probability of heterogeneity (right scale). Above baseline represents CH1-CH2 >0; below baseline represents CH1-CH2 <0.

caused by minimum expression in the control cells: the signal intensity ratio of query/control cells may have a large variation range when the expression level of genes in control cells is very low, resulting in false positive results. In fact such genes sometimes showed controversial expression changes between real-time RT-PCR and cDNA microarray with global normalization, or even among real-time RT-PCR with different internal controls (Fig. 4 and Table III; nTE4-5 strains for *SERPINB2, EGR1, EREG, TNC, LGALS3BP*, and *IGFBP5*). By the proposed normalization, such spots were judged as 'off, off' and probability of heterogeneity became low, as shown in Fig. 2 (open arrow heads in lower) and Fig. 4. Even when the expression levels in control cells are comparable, some genes still showed controversial expression changes between real-time RT-PCR and cDNA microarray with global normalization. In such cases, the probability of heterogeneity usually showed minimum values such as *TACC1* in Fig. 4. Moreover, in general, a few-fold change of the expression level does not have significant biological meaning when the expression levels are high enough in both query and control cells. These genes were judged as 'on, on' and the probability of heterogeneity also became low, as shown in Fig. 2 (arrows in upper). Thus, the novel statistical procedures we applied in this study (23), evaluating the differential expression by the probability of heterogenity, would become a powerful tool to detect the target genes beyond the limits of the range of comparisons (26) that are unavoidable in any array technology using commonly used log-ratios of the measured expression levels.

We finally identified 11 and 8 genes/ESTs upregulated or downregulated, respectively, throughout the cellular immortalization processes in fibroblast MJ90 to TF1 strains and 13 and 7 genes/ESTs in endothelial cell HUE142-2 to nTE4-5 strains among the 21,168 spots (Table II). Interestingly no commmon gene was overlapped in fibroblasts and endothelial cells. Only *BGN* (Fig. 3, arrows) and *COL5A2* (Fig. 3, open arrow heads) were detected as commonly downregulated except for in TF1 cells at PDL 104. Biglycan is a prototype member of the small leucine-rich proteoglycan family and is likely involved in the cell-specific regulation of cell proliferation and growth (27). On the contrary, biglycan was reported to inhibit growth of pancreatic cancer cells by arresting in G1, as a part of host defense mechanism aimed at slowing down pancreatic tumor progression (28). In the present study, rapid proliferating immortalized endothelial cells and fibroblasts showed continuous repression of bigrican, but not in slow growing fibroblasts, indicating that repression of bigrican may be involved in the increasing proliferative capacity of *hTERT* transfected normal human cells. Similarly, *COL5A2*, which has been reported as expressed in colon cancers but not in normal intestinal epithelia or adenomas (29), was continuously downregulated in rapid proliferating

Table III. Relative expression levels estimated by real-time RT-PCR.

	TF1-PDL				nTE4-5-PDL			
Cell	MJ90	104	148	216	HUE145-2	105	145	216
BGN/GAPD	3.10	5.76	0.15	0.02	5.17	0.11	0.43	0.00
BGN/ACTB	3.33	6.93	0.22	0.02	5.98	0.19	0.90	0.01
MMP3/GAPD	11.31	0.17	0.35	1.59	0.00	0.00	0.00	0.00
MMP3/ACTB	12.15	0.20	0.52	2.32	0.00	0.00	0.00	0.00
ALDH1A1/GAPD	2.56	4.08	0.91	0.18	1.68	0.81	0.94	0.39
ALDH1A1/ACTB	2.75	4.92	1.32	0.27	1.94	1.34	1.96	0.69
SERPINB2/GAPD	9.52	3.66	0.01	0.02	0.43	0.45	0.12	0.17
SERPINB2/ACTB	10.22	4.40	0.02	0.03	0.49	0.74	0.26	0.30
EGR1/GAPD	1.59	2.02	1.27	0.41	0.02	0.01	0.02	0.04
EGR1/ACTB	1.71	2.43	1.85	0.59	0.03	0.02	0.05	0.08
EREG/GAPD	1.13	1.52	4.77	1.79	0.00	0.00	0.00	0.01
EREG/ACTB	1.21	1.83	6.94	2.61	0.00	0.00	0.00	0.02
TNC/GAPD	8.08	1.24	2.53	0.74	0.00	0.00	0.00	0.00
TNC/ACTB	8.68	1.50	3.69	1.09	0.00	0.00	0.00	0.00
LGALS3BP/GAPD	0.91	3.77	2.76	1.23	0.11	0.09	0.06	0.14
LGALS3BP/ACTB	0.98	4.54	4.02	1.79	0.13	0.14	0.12	0.24
IGFBP5/GAPD	5.53	6.52	0.06	0.05	0.00	0.00	0.00	0.01
IGFBP5/ACTB	5.94	7.86	0.09	0.08	0.00	0.01	0.00	0.02
TACC1/GAPD	1.06	0.85	0.90	0.66	1.87	1.64	1.62	1.73
TACC1/ACTB	1.14	1.02	1.31	0.96	2.16	2.72	3.38	3.07

Relative expression level 1 = expression level using 20 ng of control total RNA mixture of the 8 cell strains. *GAPD* and *ACTB* are used as internal controls.

cellular immortalization processes. This opposite dysregulation might be related with the fact that *hTERT*-mediated cellular immortalization is a different phenomenon from carcinogenesis. These genes are the most plausible candidates to have a role in maintaining immortal capacity, but further study is necessary to draw the conclusion.

Among the remaining genes continuously dysregulated during cellular immortalization, some were related to oxidative or hypoxic stresses, such as *SOD3* and *EPAS1*. It was reported that oxidative stress induces faster telomere shortening (30) and may prevent *hTERT*-transfected fibroblasts from acquiring immortality (18). These genes may be involved in overcoming the oxidative or hypoxic stress during cellular immortalization processes. Pregnancy specific ß-1-glyco-proteins (PSBGs), such as PSG1, PSG3, PSG4, and PSG5; and gonadal protein, such as follistatin (FST), were commonly upregulated in immortalized endothelial cells. Although the functions of these proteins are still unclear, PSBGs are related to carcinoembryonic antigen (CEA) and may be involved in continuous cellular proliferation. However, a few genes showed controversial expression changes with regard to previous reports in cancer cells, such as *FABP3* (31), *MMP3* (32), *GOPC* (33), and *ERBB2* (34), as was *COL5A2* (29). The biological roles of these genes in cellular immortalization remained to be elucidated (Table II).

It is generally understood that once telomerase is activated, cancer cells would acquire immortality and would not reverse to mortal cells without artificial intervention such as induction of differentiation. Meanwhile, no normal somatic cell was shown to have naturally acquired immortality even with capacity of telomerase activation, e.g., in stem/progenitor cells of self-renewal tissues and lymphocytes. Even with ectopic expression of telomerase by transfection of *hTERT*, cellular immortalization is a rare event for normal somatic cells, and oncogenic transformation seems prerequisite for epithelial cells to acquire immortality (35,36). In fact, in the present study, we established only one immortal cell line each for fibroblasts and endothelial cells after several trials of *hTERT* transfection, and failed in epithelial cells, esophageal epithelial cells and airway epithelial cells (data not shown). These findings indicate that normal somatic cells would require cell-type specific events in addition to telomerase activation, and a rare population that eventually experience such events would acquire immortality. Telomerase activity and proliferation capacity in normal telomerase-positive somatic cells are repressed in the absence of cell proliferation stimuli or after several cell divisions, even under continuous stimuli. However, the *hTERT* expression levels and proliferation capacity in *in vitro* established immortal normal cell lines, TF1 and nTE4-5, were never repressed, as was in cancer cell lines. Considering this, the intrinsic events required for cellular immortalization in normal somatic cells might be in a mutational manner, as was likely in cancer cells, but at least some of the events might be different from those in cancer cells. And the 18 and 20 genes identified in the present study as dysregulated throughout the cellular immortalization processes in fibroblasts or endothelial

cells, respectively, may include the critically responsible genes for the events. Further functional analyses on each of these genes may elucidate the truly responsible genes in cellular immortalization. The key molecules that distinguish the mechanisms of cellular immortality of cancerous and noncancerous cells are expected to become the crucial targets for anticancer therapy and regenerative therapy.

Acknowledgements

We thank Professor F. Ishikawa for providing *hTERT* constructs and Professor J.R. Smith for MJ90 strain. We also thank Professor E. Hiyama, Ms. A. Wakamoto, Ms. C. Oda, and Ms. M. Kaneyasu, for their technical support. This study was partly supported by grant from the New Energy and Industrial Technology Development Organization, by Grants-in-Aid for Scientific Research from the Ministry of Education, Culture, Science, Sports and Technology of Japan, and for University and Industry Collaboration with Taiho Pharmaceutical Co., Ltd.

References

1. Olovnikov AM: Principle of marginotomy in template synthesis of polynucleotides. Dokl Akad Nauk 201: 1496-1499, 1971.
2. Hayflick L and Moorhead PS: The serial cultivation of human diploid cell strains. Exp Cell Res 25: 585-621, 1961.
3. Greider CW and Blackburn EH: Identification of a specific telomere terminal transferase activity in Tetrahymena extracts. Cell 43: 405-413, 1985.
4. Harley CB: Telomere loss: mitotic clock or genetic time bomb? Mutat Res 256: 271-282, 1991.
5. Kim NW, Piatyszek MA, Prowse KR, Harley CB, West MD, Ho PLC, Coviello GM, Wright WE, Weinrich SL and Shay JW: Specific association of human telomerase activity with immortal cells and cancer. Science 266: 2011-2015, 1994.
6. Hiyama K, Hirai Y, Kyoizumi S, Akiyama M, Hiyama E, Piatyszek MA, Shay JW, Ishioka S and Yamakido M: Activation of telomerase in human lymphocytes and hematopoietic progenitor cells. J Immunol 155: 3711-3715, 1995.
7. Hiyama E, Hiyama K, Tatsumoto N, Kodama T, Shay JW and Yokoyama T: Telomerase activity in human intestine. Int J Oncol 9: 453-458, 1996.
8. Ramirez RD, Wright WE, Shay JW and Taylor RS: Telomerase activity concentrates in the mitotically active segments of human hair follicles. J Invest Dermatol 108: 113-117, 1997.
9. Kyo S, Takakura M, Kohama T and Inoue M: Telomerase activity in human endometrium. Cancer Res 57: 610-614, 1997.
10. Hiyama E, Hiyama K, Yokoyama T, Matsuura Y, Piatyszek MA and Shay JW: Correlating telomerase activity levels with human neuroblastoma outcomes. Nat Med 1: 249-255, 1995.
11. Hiyama K, Hiyama E, Ishioka S, Yamakido M, Inai K, Gazdar AF, Piatyszek MA and Shay JW: Telomerase activity in small cell and non-small cell lung cancers. J Natl Cancer Inst 87: 895-902, 1995.
12. Hiyama E, Hiyama K, Yokoyama T and Shay JW: Immunohistochemical detection of telomerase (hTERT) protein in human cancer tissues and a subset of cells in normal tissues. Neoplasia 3: 17-26, 2001.
13. Bodnar AG, Kim NW, Effros RB and Chiu CP: Mechanism of telomerase induction during T cell activation. Exp Cell Res 228: 58-64, 1996.
14. Masutomi K, Yu EY, Khurts S, Ben-Porath I, Currier JL, Metz GB, Brooks MW, Kaneko S, Murakami S, De Caprio JA, Weinberg RA, Stewart SA and Hahn WC: Telomerase maintains telomere structure in normal human cells. Cell 114: 241-253, 2003.
15. Holt SE, Aisner DL, Shay JW and Wright WE: Lack of cell cycle regulation of telomerase activity in human cells. Proc Natl Acad Sci USA 94: 10687-10692, 1997.
16. Bodnar AG, Ouellette M, Frolkis M, Holt SE, Chiu CP, Morin GB, Harley CB, Shay JW, Lichtsteiner S and Wright WE: Extension of life-span by introduction of telomerase into normal human cells. Science 279: 349-352, 1998.
17. Weinrich SL, Pruzan R, Ma L, Ouellette M, Tesmer VM, Holt SE, Bodnar AG, Lichtsteiner S, Kim NW, Trager JB, Taylor RD, Carlos R, Andrews WH, Wright WE, Shay JW, Harley CB and Morin GB: Reconstitution of human telomerase with the template RNA component hTR and the catalytic protein subunit hTRT. Nat Genet 17: 498-502, 1997.
18. Forsyth NR, Evans AP, Shay JW and Wright WE: Developmental differences in the immortalization of lung fibroblasts by telomerase. Aging Cell 2: 235-243, 2003.
19. Kumazaki T, Hiyama K, Takahashi T, Omatsu H, Tanimoto K, Noguchi T, Hiyama E, Mitsui Y and Nishiyama M: Differential gene expressions during immortalization of normal human fibroblasts and endothelial cells transfected with human telomerase reverse transcriptase gene. Int J Oncol 24: 1435-1442, 2004.
20. Lindvall C, Hou M, Komurasaki T, Zheng C, Henriksson M, Sedivy JM, Bjorkholm M, Teh BT, Nordenskjold M and Xu D: Molecular characterization of human telomerase reverse transcriptase-immortalized human fibroblasts by gene expression profiling: activation of the epiregulin gene. Cancer Res 63: 1743-1747, 2003.
21. Gerhold DL, Jensen RV and Gullans SR: Better therapeutics through microarrays. Nat Genet 32 (Suppl): 547-552, 2002.
22. Quackenbush J: Microarray data normalization and transformation. Nat Genet 32 (Suppl): 496-501, 2002.
23. Ohtaki M, Otani K, Satoh K and Nishiyama M: Model-Based Analysis of Microarray Data: Exploration of Differentially Expressed Genes Between two Cell Types Based on a two-Dimensional Mixed Normal Model. Technical Report Series of Statistical Research Group, Hiroshima Univershity No. 04-07, 2004.
24. Nakayama J, Tahara H, Tahara E, Saito M, Ito K, Nakamura H, Nakanishi T, Tahara E, Ide T and Ishikawa F: Telomerase activation by hTRT in human normal fibroblasts and hepatocellular carcinomas. Nat Genet 18: 65-68, 1998.
25. Tanaka T, Tanimoto K, Otani K, Satoh K, Ohtaki M, Yoshida K, Toge T, Yahata H, Tanaka S, Chayama K, Okazaki Y, Hayashizaki Y, Hiyama K and Nishiyama M: Concise prediction models of anticancer efficacy of 8 drugs using expression data from 12 selected genes. Int J Cancer 111: 617-626, 2004.
26. Sharov V, Kwong KY, Frank B, Chen E, Hasseman J, Gaspard R, Yu Y, Yang I and Quackenbush J: The limits of log-ratios. BMC Biotechnol 4-3, 2004.
27. Shimizu-Hirota R, Sasamura H, Kuroda M, Kobayashi E, Hayashi M and Saruta T: Extracellular matrix glycoprotein biglycan enhances vascular smooth muscle cell proliferation and migration. Circ Res 94: 1067-1074, 2004.
28. Wever CK, Sommer G, Michl P, Fensterer H, Weimer M, Gansauge F, Leder G, Adler G and Gress TM: Biglycan is overexpressed in pancreatic cancer and induces G1-arrest in pancreatic cancer cell lines. Gastroenterology 121: 657-667, 2001.
29. Fischer H, Stenling R, Rubio C and Lindblom A: Colorectal carcinogenesis is associated with stromal expression of COL11A1 and COL5A2. Carcinogenesis 22: 875-878, 2001.
30. Kurz DJ, Decary S, Hong Y, Trivier E, Akhmedov A and Erusalimsky JD: Chronic oxidative stress compromises telomere integrity and accelerates the onset of senescence in human endothelial cells. J Cell Sci 117: 2417-2426, 2004.
31. Huynh H, Alpert L and Pollak M: Silencing of the mammary-derived growth inhibitor (MDGI) gene in breast neoplasms is associated with epigenetic changes. Cancer Res 56: 4865-4870, 1996.
32. Sternlicht MD, Bissell MJ and Werb Z: The matrix metalloproteinase stromelysin-1 acts as a natural mammary tumor promoter. Oncogene 19: 1102-1113, 2000.
33. Charest A, Lane K, McMahon K, Park J, Preisinger E, Conroy H and Housman D: Fusion of FIG to the receptor tyrosine kinase ROS in a glioblastoma with an interstitial del(6)(q21q21). Genes Chromosomes Cancer 37: 58-71, 2003.
34. Menard S, Pupa SM, Campiglio M and Tagliabue E: Biologic and therapeutic role of HER2 in cancer. Oncogene 22: 6570-6578, 2003.
35. Hahn WC, Counter CM, Lundberg AS, Beijersbergen RL, Brooks MW and Weinberg RA: Creation of human tumour cells with defined genetic elements. Nature 400: 464-468, 1999.
36. Lundberg AS, Randell SH, Stewart SA, Elenbaas B, Hartwell KA, Brooks MW, Fleming MD, Olsen JC, Miller SW, Weinberg RA and Hahn WC: Immortalization and transformation of primary human airway epithelial cells by gene transfer. Oncogene 21: 4577-4586, 2002.

Molecular and Biological Heterogeneity in Neuroblastoma

Eiso Hiyama[1,*] and Keiko Hiyama[2]

[1]Natural Science Center for Basic Research and Development and [2]Department of Translational Cancer Research, Research Institute for Radiation Biology and Medicine, Hiroshima University, 1-2-3 Kasumi, Minami-ku, Hiroshima, 734-8551, Hiroshima, Japan

Abstract: Neuroblastoma, one of the common malignant childhood tumors, arises from neuroblast cells derived from the neural crest and destined for the adrenal medulla and the sympathetic nervous system and shows remarkable biological heterogeneity, resulting in favorable or unfavorable outcomes. Some neuroblastomas tend to regress spontaneously in infants or to differentiate into a benign ganglioneuroma in older patients. In other instances, the tumors make rapid progress with a fatal outcome. This heterogeneity within neuroblastoma depends on the molecular characteristics of tumor cells. Several distinct genomic alterations have been found in neuroblastoma, including *MYCN* amplification, ploidy changes, deletion of the short arm of chromosome 1, gain of chromosome 17q, and deletion of 11q. The difference of expression was also found in genes related to cellular growth, differentiation, and apoptosis of neural network including Trk receptor tyrosine kinase and telomerase activity. This review discusses the extensive heterogeneity of neuroblastoma at molecular level, providing evidences that neuroblastoma is not a single disease. This should lead to more risk-adapted therapies according to the genetic markers by which individual neuroblastomas are biologically characterized.

Received on: 06 May 2005 - Accepted on: 08 June 2005

Key Words: Neuroblastoma, prognosis, *MYCN*, ploidy, chromosome, telomerase, telomere, apoptosis.

INTRODUCTION

Neuroblastoma, which is derived from neuroectodermal cells in neural crest, is the most common malignant solid tumor in children. The incidence of neuroblastoma is about 1 case per 7, 000 born babies a year [1]. More than 90% of children with neuroblastoma are diagnosed within the first 5 years of age, typically characterizing an embryonic tumor. Neuroblastoma exhibits three distinct patterns of clinical behavior: life-threatening progression, spontaneous regression and maturation to ganglioneuroma. Many patients who are diagnosed at more than one year of age have advanced neuroblastomas with metastasis which are usually associated with poor outcome despite multimodal therapy. On the other hand, some tumors undergo complete regression without any treatment. Spontaneous regression usually occurs as part of a clinically identified entity designated stage 4S which has a primary tumor localized in the adrenal gland and metastasis restricted in the liver, bone marrow, and/or skin [2-4]. Maturation to benign ganglioneuroma is less frequent and usually observed after chemotherapy. Although spontaneous regression mainly occurs in infants, maturation is well described in older patients [5]. Since more than 80% of neuroblastomas produce catecholamine metabolites (vanillylmandelic acid and homovanillic acid) are detectable in the urine, mass-screening projects to detect earlier stages of neuroblastoma have been carried out in some countries including Japan. Surprisingly, the incidence of this disease increased two fold whereas the incidence of advanced neuroblastoma in older patients did not changed remarkably, indicating that a large number of neuroblastomas occur in infants without clinical detection and spontaneously regress or mature behind the scenes. These projects were not so effective to reduce progressive neuroblastoma but gave us a lot for solving the biological problem in neuroblastoma. [6-8]. These phenomena raised the question whether advanced stage tumors develop from early stage tumors or represent a subgroup. Transition from favorable type to unfavorable type has not been clearly evaluated but seems to occur rarely [9], suggesting that neuroblastoma consist of at least more than two distinct subtypes [10], which may be distinguishable by genetic characteristics.

These clinical findings suggest biological heterogeneity of neuroblastoma: some tumors regress or mature and other instances advance aggressively. To distinguish progressive tumors from favorable tumors is needed because multimodal appropriate therapies are necessary to improve the prognosis of the patients with progressive tumors and aggressive therapy should be avoided in the patients with favorable tumors to reduce side effects and cost. Clinical evaluation for this difference is based on stage of disease (the degree of tumor spread) at diagnosis, age at diagnosis, histological classification, and only more recently several biological markers have been incorporated [11]. Histological classification by Shimada *et al.* according to the degree of ganglionic differentiation and Schwannian stroma has been widely accepted as an important prognostic factor [12, 13].

To identify the molecular and biological heterogeneity of neuroblastoma clearly, numerous multilateral approaches have been performed for the past two decades and several distinct alterations have been found including *MYCN* amplification, ploidy, chromosomal loss and gain, expression of

*Address correspondence to this author at the Natural Science Center for Basic Research and Development, Hiroshima University, 1-2-3 Kasumi, Minami-ku, Hiroshima, 734-8551, Hiroshima, Japan; Tel: +81-82-255-5951, Fax: +81-82-257-5219; E-mail: eiso@hiroshima-u.ac.jp

1389-2029/05 $50.00+.00

Trks, and telomerase activity. In this review, the extensive heterogeneity of neuroblastoma was summarized at molecular and biological evidences that neuroblastoma is not a single disease. This should lead to more risk-adapted therapies according to the genetic markers by which individual neuroblastomas are biologically characterized. This approach will lead to find the molecular marker to distinguish progressive tumors at diagnosis as well as the molecular targets to treat these tumors. In addition, it will provide insights into mechanisms of malignant transformation, progression, spontaneous regression and maturation in neuroblastoma.

BIOLOGICAL AND MOLECULAR MARKERS

MYCN Amplification

Amplified *MYCN* is one of the most distinguished genomic aberrations of neuroblastomas. Cytogenetic analysis of neuroblastoma cells with amplified *MYCN* gene showed chromosomal abnormalities such as homogeneously staining regions (HSRs) or double minutes (DMs). DMs are usually detected in primary tumors and HSRs which are generally located on different chromosomes from the resident site 2p24 of *MYCN*, were found in cell lines with amplified *MYCN* (Fig. (1)) [14, 15].

Amplified *MYCN* was observed in half of advanced neuroblasotmas, but was hardly detected in early stage tumors [14, 15]. In patients who have the tumors with non-amplified *MYCN*, overall survival was approximately 60% over a 5-year period, but less than 30% of patients survived a 1-year period when *MYCN* was amplified at more than ten copies [9, 11]. Thus, amplified *MYCN* is established as a powerful clinical marker of high-risk neuroblastoma and the only tumor genetic marker used as a basis for treatment stratification in neuroblastoma clinical trials [16-19]. Recent studies revealed that the patients who have tumors with amplified *MYCN* gene between three and nine copies also showed poor outcomes [20, 21]. Moreover, FISH analyses of primary tumors for detection at the single cell level revealed that individual cells from *MYCN*-amplified tumors typically stray widely from the copy numbers estimated by molecular analyses (Fig. (1)) [20, 22]. These suggested that amplified *MYCN* gene characterizes a subset of neuroblastoma with extremely aggressive growth potential regardless of the copy number of *MYCN* gene.

The copy numbers of amplified *MYCN* gene, which ranges between three-fold and more than 500-fold, is considered to be consistent within a tumor; not only at different tumor sites, but also at different times *in vivo* [23]. This suggests that amplified *MYCN* is generally present at the time of diagnosis. However, there are some evidences that the *MYCN* gene is amplified during progression of neuroblastoma [24]. Our distinguished case which had the rearrangement in the half copies of amplified *MYCN* gene in one of metastatic lesions suggested that the *MYCN* amplification occurred during tumor progression [25]. In the majority of cases amplified *MYCN*, 1p deletion and 17q gain coexist in the same tumors. Amplified *MYCN* rarely, if ever, occurs without either 1p deletion or 17q gain or both. These phenomena imply that *MYCN* amplification is a later event in the sequence of genetic aberrations underlying neuroblastoma progression [26].

The size of amplicon with amplified DNA encompassing *MYCN* ranges from 100 kb to more than 1 Mb [27], suggesting the possibility that additional genes are co-amplified. *DDX1* gene and neuroblastoma amplified gene (*NAG*) were reported to be coamplifed in 50-70% of the tumors with *MYCN* amplification but no amplification of *DDX1* or *NAG* without concomitant *MYCN* amplification has been reported, indicating that *MYCN* is functionally responsible for the maintenance of the amplicon.

High levels of *MYCN* expression are observed in *MYCN*-amplified tumors and seem to contribute to tumorigenesis. However, there are conflicting reports regarding the potential prognostic significance of expression products, both mRNA and protein. Whereas one study demonstrated no significant correlation of *MYCN* expression and MYCN protein levels with patient prognosis [28], others reported that in patients older than 1 year with *MYCN* non-amplified tumors, high levels of *MYCN* expression are associated with poor outcome [29, 30].

DNA Ploidy

Cytogenetic and flow cytometric analyses have been used for evaluating DNA ploidy in neuroblastoma. Flow cytometric analysis revealed that hyperdiploidy, mostly the near-triploidy, is mainly observed in favorable tumors of younger patients, whereas diploid is usually detected in advanced tumors with unfavorable outcomes [31]. In addition, in children 12-24 months of age, diploidy predicted resistance for chemotherapy, whereas half of the patients with hyperdiploidy achieved long-term disease-free survival. The DNA ploidy did not have its prognostic significance for patients over 2 years of age [32].

Cytogenetic analyses classified neuroblastoma tumors into four ploidy patterns: near-diploid, near-triploid, near-tetraploid, and near-pentaploid tumors [33]. The near-diploid and near-tetraploid tumors were usually detected in children older than 1 year and frequently had genetic abnormalities involving 1p and *MYCN* amplification. On the other hand, near-triploid and near-pentaploid tumors were predominantly detected in infants with favorable outcome and rarely showed genetic abnormalities. Near-diploidy and near-tetraploidy have been identified as one of the most useful markers for poor prognosis [34].

Using two-color FISH for observing 1p deletion and ploidy in tumors in Japan where mass-screened program had been performed [33], event-free survival (EFS) rate was lowest in the disomy 1 with 1p deletion group, intermediate in the disomy 1 with normal 1p group and highest in both trisomy 1 regardless 1p status. This indicates that cytogenetic 1p deletion is a poor prognostic factor for diploid tumors, but not for triploid tumors. The majority of trisomy 1 tumors with 1p36 deletion were detected by mass screening.

Chromosome Loss and Gain

Chromosome loss and gain in neuroblastoma were reported in more than 20 different chromosome regions, most frequently chromosome 1, followed by 11q, and 17q. More recently CGH analyses have substantially contributed to the identification of unbalanced 17q gain in primary neuroblastoma [35-37].

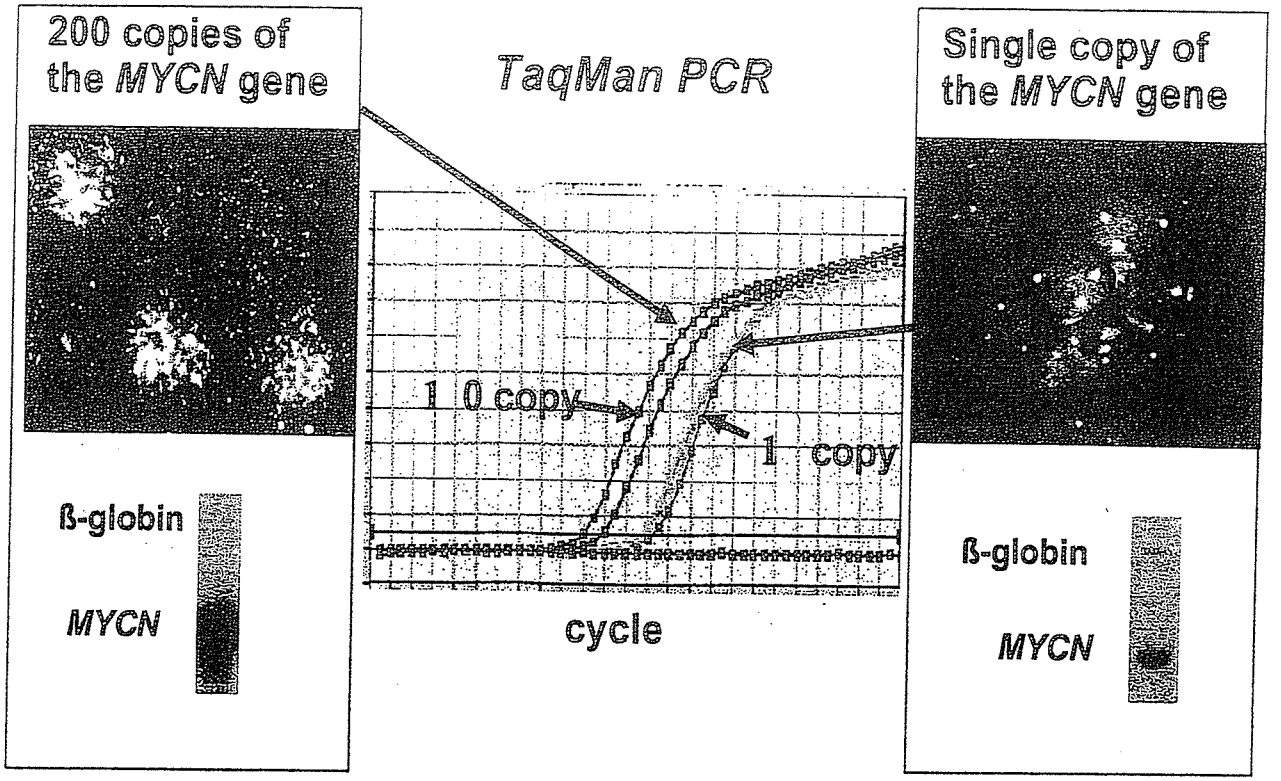

Fig. (1). Detection of *MYCN* amplification in neuroblastoma. *MYCN* copy number is usually determined by Southern blot, quantitative real time PCR (TaqMan®), or fluorescence *in situ* hybridization.

Several reports demonstrated that chromosome 1p deletion occurs in approximately 35% of all neuroblastomas [38, 39] and a smallest region of overlapping deletion (SRO) was mapped to 1p34-p36 [40], suggesting that tumor suppressor genes for the development of neuroblastoma might be located in this region. Recently, the SRO was refined to a size of approximately 1 Mb within 1p36.3, which was defined by the region of LOH in a primary tumor that extends distally from *DIS214*. Patients whose tumors had large 1p deletions showed poorer outcome than patients with short or interstitial deletions [41, 42], suggesting the existence of more than one deleted 1p loci in neuroblastoma. The tumors with large 1p deletions were associated with adverse prognostic factors, such as diploidy or tetraploidy and amplified *MYCN*, while the tumors with small interstitial deletions of 1p associated with triploidy in favorable tumors. The regions of 1p deletions of *MYCN*-amplified tumors are very large including a region from 1p32 to telomere [24]. In contrast, in single-copy *MYCN* cases, 1p deletions were described to be consistently smaller, and a commonly deleted region maps to 1p36.1. Thus, the second tumor suppressor gene, which is correlated with progressive neuroblastoma, was suggested to be localized at proximal (1p32) or distal (1p36.3) to the deletion border of the smallest 1p deletion found in single-copy *MYCN* tumors [43, 44]. The SRO of the single-copy *MYCN* tumors is included in the larger SRO of *MYCN*-amplified tumors, implying that more than two suppressor loci in 1p must be simultaneously deleted in *MYCN*-amplified tumors.

Preferential deletion of the maternal allele in single copy *MYCN* tumors [45] would imply that the distal locus of tumor suppressor gene (TSG) at 1p36.3 may be subject to genomic imprinting. Recent study indicated that the origin of the affected allele is frequently parental of random distribution in neuroblastoma with a large 1p deletion and in amplified *MYCN* gene [46]. Now, the reports for preferential loss of the allele have given conflicting results [43, 45, 47, 48].

Thus, the biological effect of 1p deletions has remained unclear. Several candidate TSGs have been proposed, but none has been shown to contain tumor-specific mutations, indicating that alternate mechanisms of TSG inactivation, such as epigenetic mechanisms of gene inactivation or haploinsufficiency, also have to be considered. 1p alterations are frequently detected together with other genetic alterations, such as amplified *MYCN*, 17q gain, diploidy/triploidy, and each combination appears to have a divergent impact on tumor growth characteristics. In the recent study, LOH at 1p36 was a significant independent predictor of decreased event-free survival, but had no significant effect on overall survival in multivariate analysis [49]. In contrast, amplified *MYCN* was a more powerful prognostic factor for decreased overall survival. This implies that 1p36 allelic status may be useful for predicting which neuroblastoma patients with otherwise favorable clinical and biological features are more likely to have disease progression. Closer surveillance is needed after surgery for disease progression because these patients can be salvaged with additional therapy.

Cytogenetic studies also revealed additional copies of 17q in cell lines and primary tumors [50]. Several studies of neuroblastoma cells and tumors have indicated a high frequency of unbalanced translocations involving chromosome

17q [30, 51, 52]. Clinically, gain of 17q is more common at an advanced stage, in tumors from children aged over 1 year, and in tumors showing 1p loss, *MYCN* amplification and diploidy/ tetraploidy. On the other hand, triploidy with whole chromosome 17 gain is associated more often with neuroblastomas showing favorable clinical features [26]. The report from six European centers with more than 300 cases identified that 17q gain was the most powerful prognostic factor of survival in multivariate analysis with other clinical and tumor genetic parameters, including 1p deletion and *MYCN* amplification. In stepwise multivariate analysis, significant independent predictors of lethal outcome were 1p deletion ($P = 0.02$), stage 4 disease ($P = 0.004$), and 17q gain ($P < 0.001$) [26]. These studies suggested that unbalanced gain of distal 17q is the independent prognostic factor for predicting high risk for tumor progression and that the region of chromosome 17q gain includes a gene critical for tumor progression. FISH analyses indicated that the breakpoints were clustered in the proximal half of 17q from *D17Z1* to *MPO* (17q23.1), with a shortest region of gain extending from *MPO* to 17qter [53, 54]. Several candidate genes have been proposed to be responsible for the 17q-gain effect on tumor growth characteristics. Survivin, an anti-apoptosis protein, which was recently mapped to 17q25, is one candidate as its expression correlates strongly with adverse clinical data [55]. *NM23-H1* located at 17q21-22 is another candidate because overexpression of nm23-H1 has been demonstrated in aggressive neuroblastoma tumors [56, 57].

Cytogenetic analyses have also reported 11q deletion in about 15% of neuroblastomas [58]. Constitutional rearrangements of 11q have been reported in some neuroblastoma patients, including a deletion of 11q23-qter, [59-61]. These constitutional changes may predispose paitents to the development of neuroblastoma. On the other hand, LOH studies revealed 11q loss in 5-32% of the tumors [62-64]. Loss of the whole chromosome 11 was observed in 19%, while unbalanced 11q LOH was observed in 22% of primary neuroblastomas [65]. Loss of the whole chromosome 11 was mainly detected in low stage tumors, whereas unbalanced deletion of 11q was predominantly detected in high stage tumors without amplified *MYCN* [65, 66]. Loss of 11q was significantly correlated with adverse clinical parameters, including age over 1 year, stage 4 tumors and unfavorable histology [67]. The SRO in 11q23.3 is between markers *D11S1340* and *D11S1299* in the tumors with 11q LOH [66]. Unbalanced 11q deletion is considered as a frequent event in the *MYCN* non-amplified tumors and COG study recently revealed that 11q deletion is an independent prognostic indicator for predicting high risk for tumor progression, especially in *MYCN* non-amplified tumors [35, 68].

Recently, genome-wide linkage analysis revealed that a candidate locus for the gene has been localized to chromosome band 16p12 [69, 70] in familial neuroblastomas [71], whereas other loci, such as chromosome 1p, have been excluded [49, 72]. Although a familial neuroblastoma predisposition gene would function as a tumor suppressor, it is possible that dominant mutations may predispose to neuroblastoma.

Representational difference analysis (RDA) revealed that the most frequently deleted region, apart from 1p, was chromosomal region 3p [73]. In this study, a SRO encompassing chromosome bands 3p25.3-p14.3 with 46 cM was defined [74]. Recently, a novel 3p21.3 candidate tumor suppressor, a *RAS* association domain family protein (*RASSF1A*), which was identified within the SRO [75], has been shown to be epigenetically silenced by promoter methylation in primary neuroblastomas and other cancer types[76]. Silencing of *RASSF1A* may contribute to aberrations of *RAS* signal pathways observed in neuroblastomas [77]. In addition, a significant correlation between *RASSF1A* and *CASP8* methylation in neuroblastoma was demonstrated [76], suggesting that some neuroblastomas may have a CpG island methylator phenotype.

Recently, comparative genome hybridization (CGH) has been used for genome-wide screening of gains and losses in neuroblastoma [35-37, 78]. With respect to ploidy changes in neuroblastoma, CGH analyses have confirmed the findings of flow cytometry and classical cytogenetic analysis: triploid tumors with favorable outcomes are characterized by numerical chromosome imbalances with only few structural abnormalities, including the typical pattern of gains for chromosomes 1, 2, 6, 7, 8, 12, 13, 17, 18, and 22, and losses for chromosomes 3, 4, 9, 11, 14, and X [37]. Partial loss of the chromosomes is usually detected in advanced stage tumors. Similarly, gain of the whole chromosome 17 is predominantly observed in low stage tumors, whereas partial gain of 17q is usually detected in advanced stage tumors [37]. A number of CGH studies have also confirmed the unbalanced 11q deletion in approximately 20% of primary neuroblastomas, and loss of whole chromosome 11 was a frequent finding in near-triploid low stage neuroblastomas [35, 78, 79]. Unbalanced 11q deletion was detected in more than 50% of stage 4 neuroblastomas without *MYCN* amplification [35]. This genetic subgroup is also characterized by a positive correlation with deletion events, such as losses of 3p, 4p, and 14q, and an inverse correlation with 1p deletion, and furthermore 17q gain was consistently present [35, 37]. More recently, array-based CGH, a powerful tool for survey whole chromosomal changes in the tumor cells, revealed that major alternations in neuroblastoma cells are loss of 1p, 11q, and gain of 17q [80]. Array-based CGH and SNPs array have been developed for gemone-wide screening at approximately 1 Mb and 100 Kb mapping resolution, respectively. These methods will clarify the genetic differences between these two groups in future.

Allelic Loss and Tumor Suppressor Genes (TSGs)

In addition to amplified *MYCN* gene, 1p deletion, 17q gain, 11q deletion, and ploidy changes, further genetic alterations exist in neuroblastomas (Table (1)). In general, deletions are more common than defined chromosomal gains in neuroblastoma. Molecular genetic characterization of deleted regions in neuroblastoma largely depends upon the two-hit hypothesis [81], predicting that LOH events are the second step in the inactivation of both alleles of a TSG. LOH analyses in a large number of cases were used to define a shortest region of overlapping region (SRO) containing one or more putative TSGs. In the chromosome 1p, the numerous researches have been performed and the SRO in 1p has been narrowed into 1p36 region [24, 41, 42, 49, 63, 72]. The number of candidate genes that have emerged from LOH analyses is small, but none has been identified as the classi-

cal TSG in neuroblastoma. There may be several explanations as follows: (1) Chromosomal instability, which especially occurs in advanced stage neuroblastomas, frequently causes marker chromosomes and unidentified products of unbalanced translocations. This chromosomal instability may increase the rate of LOH, and it seems possible that not all of these LOH events are critical for tumor progression. (2) LOH could result in haploinsufficiency and the reduced activity of a particular gene at a given locus, alone or in combination with other genes, could contribute to tumorigenesis. (3) Epigenetic mechanisms such as silencing, could play an important role for tumorigenesis, then mutation is undetectable in the loci of LOH.

Table 1. Genetic and Molecular Abnormalities in Neuroblastoma

Abnormalities	Associated genetic/ molecular abnormalities	Prognosis
Triploid/ pentaploid	Unknown	Good
Diploid/ tetraploid	*MYCN* amplification	Poor
LOH 1p	*MYCN* amplification	Poor*
LOH 3p	LOH 11q, 14q, *MYCN* normal	Intermediate
LOH 4p	Unknown	Unknown
LOH 9p	Unknown	Unknown
LOH 11q	LOH 3p, 14q, *MYCN* normal	Intermediate
LOH 14q	LOH 3p, 11q, *MYCN* normal	Intermediate
17q gain	t(1;17) or t(11; 17)	Poor
	NM23-H1 overexpression	
	Survivine overexpression	
	MYCN amplification	
MYCN amplification	LOH 1p, 17q gain	Poor
CCND1 amplification	*CCND1* overexpression	Unknown

LOH, Loss of heterozygosity

*1p 36 small deletion is not correlated with poor prognosis

The *TP53* gene is one of the most famous TSGs in human neoplasia. Several studies have examined TP53 gene mutation but it was rare in neuroblastoma [82]. However, there is still controversy about this involvement of TP53 in neuroblastoma. Some reports showed cytoplasmic sequestration in undifferentiated neuroblastoma [83], whereas p53 mutations develop frequently in relapsed neuroblastoma, correlating with multi-drug resistance [84, 85]. The *CDKN2A* (INK4A/p16) gene is sometimes deleted or mutated in adult cancers, while inactivation of this gene has not been reported in primary neuroblastoma [86].

Apoptosis related genes have been emerged as one of the strongest candidate TSGs in neuroblastoma. Caspase 8, a cysteine protease involved in death-receptor induced apoptosis, is activated in programmed cell death. Alterations of the caspase 8 gene, *CASP8*, have been described in neuroblastomas [87-89]. Activated caspase 8 will lead to activation of pro-caspase 3 and initiation of the final pathway to apoptosis. *CASP8* is located at human chromosome band 2q33, a region associated with LOH in neuroblastomas and several other tumor types [39, 87, 90]. The overall loss of *CASP8* expression in neuroblastomas is estimated at 25–35%, predominantly in high-risk tumors, and seems strongly associated with amplified *MYCN* [87, 88]. The lack of *CASP8* expression was associated with hypermethylation of its promoter region in neuroblastoma tumor samples. *CASP8* acts as a tumor suppressor gene, and inactivation will result in cell survival because it exists in the central position of the extrinsic apoptotic route. Tumor cells with loss of *CASP8* do not respond to TNF-receptor mediated triggers like TNF receptor apoptosis inducing ligand (TRAIL) or Fas ligand (FasL) [87, 91, 92]. Therefore, the down-regulation of *CASP8* may be the first evidence of alterations in apoptosis in neuroblastomas. Flice inhibitory protein (FLIP), a caspase 8-related protein, is an important regulator of caspase 8. The *FLIP* gene is a structural homologue of *CASP8* and co-localizes at chromosomal band 2q33. In neuroblastoma cell lines, a strong association was found between silencing of *CASP8* and *FLIP*. The majority of these cell lines were hypermethylated for *Casp8* and *FLIP* [93].

Expression of Neurotrophin Receptors

Neuroblastoma originates from sympathetic neurons, which are derived from the neural crest. The migration of neural crest cells during embryonic development is controlled by several molecules including the bone morphogenetic proteins, MASH1 (mammalian Achaete-Scute homolog 1), Ret, MYCN, and Trk family tyrosine kinase receptors. Trk receptors encoding the high-affinity receptor tyrosine kinases for neurotrophins are important to regulate growth, differentiation and apoptosis of neuroblastoma. High expression of TrkA, a high affinity receptor of NGF, which is expressed in cells at the late stage of embryonic development of sympathetic neurons, was observed in neuroblastomas with favorable prognosis which often showed spontaneous regression or maturation [94-97]. A trophic theory is that normally developing sympathetic neurons survive and differentiate by the target-derived supplement of neurotrophins. The stromal cells such as schwannian cells and fibroblasts, may supply a limited amount of NGF which partly regulates differentiation and programmed cell death of the neuroblast as shown in normal sympathetic neurons [98]. Thus, in neuroblastomas with good prognosis, tumor cells expressing TrkA receptor may be dependent on a limited amount of NGF supplied from the stromal cells and the tumor cells, when they could obtain enough amount of NGF, become to maturate or to regress spontaneously [98, 99]. On the other hand, the levels of TrkA expression are extremely low in aggressive tumors with *MYCN* amplification and/or 1p loss [94, 99]. In contrast, TrkB is preferentially expressed in aggressive neuroblastomas and its preferred ligands, BDNF and NT-4/5, are also expressed together with an autocrine/ paracrine manner [100, 101]. Thus, aggressive neuroblastomas shut off TrkA signals by down-regulating its expression or disturbing the downstream signaling cascades, whereas BDNF or NT-4/TrkB autocrine system may stimulate to grow much efficiently. TrkC is expressed rather in favorable neuroblastomas at variable levels [102], but its preferred ligand, *NTF3*, is usually undetectable by RT-PCR in primary tumors [98]. Thus, expression levels of Trks show one of heterogeneous characteristics in neuroblastoma.

Telomere and Telomerase Biology

Normal cells have a limited life span, only dividing 20 to 80 times before undergoing growth arrest (senescence) and

eventually dying. Telomere, specialized DNA-protein structure at the ends of eukaryotic chromosomes, consists of a large number of tandem repeats of short guanin-rich sequence which is highly conserved throughout evolution [103, 104]. The gradual erosion with each cell division of chromosomal telomeres plays an integral role in cell senescence and activation of a mechanism for maintaining telomeres is a key to cell immortality [105]. Telomerase is a unique reverse transcriptase capable of maintaining telomere length that is expressed in germ-line cells and immortal cells, not in most somatic cells, due to the repression of telomerase during development. Expression of telomerase activity and stabilization of telomeres are frequently found in malignant cells, which is consistent with the hypothesis that telomere maintenance is essential for attainment of immortality in tumor cells (Fig. (2)) [106, 107]. Using a highly sensitive, polymerase chain reaction-based assay for measuring telomerase activity [108, 109], which is known as the TRAP (telomeric repeat amplification protocol) assay, several studies have reported telomerase activity in neuroblastoma tissue (Table (2)) [79, 110-113]. Telomerase activity was not detectable in adrenal gland or in ganglioneuromas, but was detectable in almost all untreated neuroblastoma specimens except for stage 4S tumors [110, 111]. Moreover, high expression of telomerase activity has been shown to correlate with advanced stages of disease and with tumor biological features that predict an adverse prognosis [110-112, 114].

TRF (terminal restriction fragment) length, an indicator of telomere length, of normal adrenal glands in neuroblastoma patients ranged between 8 and 15 kb [114, 115], which are similar in size to other normal somatic cells.

Neuroblastomas with high telomerase activity have various telomere lengths, but these are presumably stabilized and maintained at a constant length, and in some cases are elongated far beyond that detected in normal cells (Fig. (3)). On

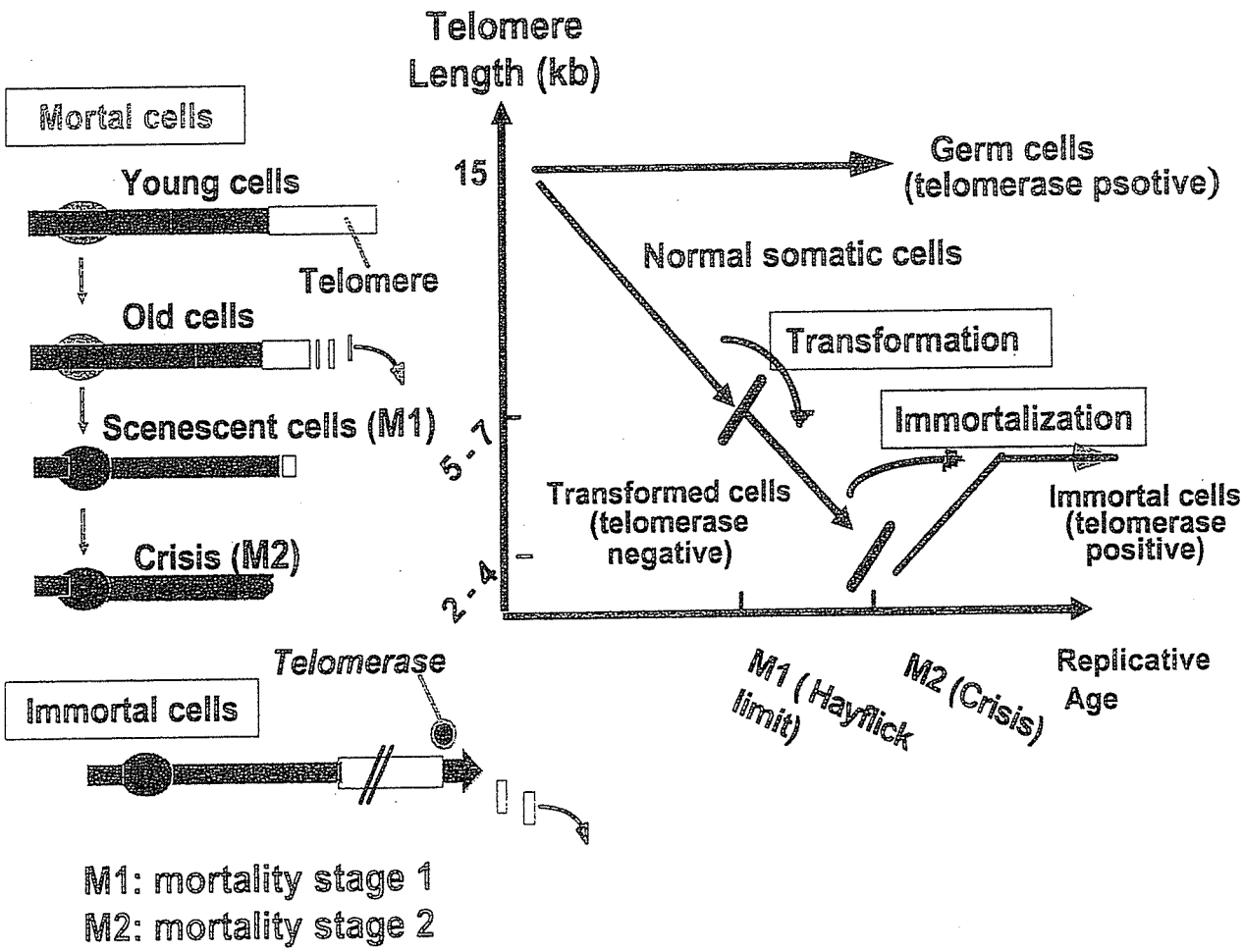

Fig. (2). The telomere hypothesis. These diagrams show the changes that occur in telomere length (vertical axis) in cells undergoing many cycles of division (horizontal axis). Human germ cells express high levels of telomerase and thus are able to keep their telomere lengths approximately 15 kilobases (kb). Germ cells differentiate into somatic cells, which do not express telomerase or do so at very low levels. Each time somatic cells divide, their telomeres shorten. When telomere attrition becomes critical (~4 kb), somatic cells senesce and can no longer divide. Telomere shortening in normal somatic cells leads to senescence which is likely triggered by a DNA damage response due to critical telomere loss or uncapping on one or a few chromosome ends (M1: mortality stage 1). If cells lack this checkpoint, or suffer a transforming growth control mutation, they can continue to divide, losing telomeric DNA until the crisis phase characterized by major telomere dysfunction, genetic instability (M2: mortality stage 2). Immortal cancer cells overcome M1 and M2 by maintaining their telomeres by the expression of telomerase. Immortal cancer cells with telomerase activity typically have short but maintained telomeres after more than 300 times replication.